Great Barrier Reef Degradation, Sea Surface Temperatures, and Atmospheric CO2 Levels Collectively Exhibit a Stochastic Process with Memory

Allan Elnar
University of San Carlos - Talamban Campus
Christianlly Cena
University of San Carlos - Talamban Campus
Christopher Casenas Bernido (cbernido.cvif@gmail.com)
Central Visayan Institute Foundation https://orcid.org/0000-0002-9329-214X
M. Victoria Carpio-Bernido
Central Visayan Institute Foundation

Research Article

Keywords: Ecological memory, Non-Markovian white noise analysis, Atmospheric CO2 levels, Great Barrier Reef, Sea surface temperatures, Anomalous diffusion

Posted Date: March 15th, 2021

DOI: https://doi.org/10.21203/rs.3.rs-299051/v1

Great Barrier Reef Degradation, Sea Surface Temperatures, and Atmospheric CO_2 Levels Collectively Exhibit a Stochastic Process with Memory

Allan R. B. Elnar [1,3], Christianlly B. Cena [1], Christopher C. Bernido [1,2,*] and M. Victoria Carpio-Bernido [1,2]

[1] *Physics Department, University of San Carlos, Talamban, Cebu City 6000, Philippines*
[2] *Research Center for Theoretical Physics, Central Visayan Institute Foundation, Jagna, Bohol 6308, Philippines*
[3] *Chemistry and Physics Department, Cebu Normal University, Cebu City 6000, Philippines*

Abstract

Quantifying ecological memory could be done at several levels from the rate of physiological changes in an ecosystem all the way down to responses at the genetic level. One way of unlocking the information encoded in a collective environmental memory is to examine the recorded time-series data generated by different components of an ecosystem. In this paper, we probe into the case of the Great Barrier Reef (GBR) which is threatened by elevated sea surface temperatures (SST) and ocean acidification attributed to rising atmospheric CO_2 levels. Specifically, we investigate the interrelated dynamics between the degradation of the GBR, SST, and rising atmospheric CO_2 levels, by considering three datasets: (a) the mean percentage hard coral cover of the GBR from the archives of the Australian Institute of Marine Science; (b) SST close to the GBR from the National Oceanic and Atmospheric Administration; and (c) the Keeling curve for atmospheric CO_2 levels measured by the Mauna Loa Observatory. We show that fluctuating observables in these datasets have the same memory behavior described by a non-Markovian stochastic process. All three datasets show a good match between empirical and analytical mean square deviation. An explicit analytical form for the corresponding probability density function is obtained which obeys a modified diffusion equation with a time dependent diffusion coefficient. This study provides a new perspective on the similarities of and interaction between the GBR's declining hard coral cover, SST, and rising atmospheric CO_2 levels by putting all three systems into one unified framework indexed by a memory parameter μ and a characteristic frequency ν. The short-time dynamics of CO_2 levels and SST fall in the superdiffusive regime, while the GBR exhibits hyperballistic fluctuation in percent coral cover with the highest values for μ and ν.

Keywords: Ecological memory • Non-Markovian white noise analysis • Atmospheric CO_2 levels • Great Barrier Reef • Sea surface temperatures • Anomalous diffusion.

1 Introduction

Ecological memory where past events shape and alter future evolution of ecosystems in a changing environment has been a recurring theme in understanding the response of an ecological community to climate change (Hughes et al 2019; Schweiger et al 2018; Peterson 2002; Ogle et al 2015; Nyström and Folke 2001; Johnstone et al 2016). An investigation of the Great Barrier Reef (GBR) demonstrated such memory in the mass coral bleaching that occurred in 2016 and 2017

* Corresponding Author: cbernido.cvif@gmail.com

(Hughes et al 2019). Memory can play an ancillary role as an ecosystem acclimatizes and develops resilience when subjected to recurring climate extremes where adaptation for coral reefs can occur even at the genetic level (Thomas and Palumbi 2017; Romero-Torres et al 2020; Carballo-Bolaños et al 2020; Mumby and van Woesik 2014; Sully et al 2019; Jurriaans and Hoogenboom 2019; Fine et al 2019; Davidson 2019). The importance of climate memory was, in fact, underscored as being crucial in determining tipping points or critical transitions in climate-sensitive systems (van der Bolt et al 2018; Turner et al 2019). Oceans, as grand matrix of ecosystems, have a perceived slow dynamics and long memory (Payne MR et al 2017). A manifestation of environmental memory of a reef coral was also observed in a ten-year study in Phuket, Thailand (Brown et al 2015). Much earlier, ecological memory was investigated in relation to a reef matrix functional diversity to maintain itself following anthropogenic disturbances (Nyström and Folke 2001). Climate predictions also depend on climate memory embodied in multi-year recorded events that capture the past needed in fine-tuning computational models to improve forecasting reliability (Corti et al 2012; Davini et al 2017; Yuan et al 2019). In this paper, we use a stochastic process with memory to provide a common analytical framework in capturing ecological memory as an interconnected phenomenon between the rising atmospheric CO_2 levels, an elevated sea surface temperature (SST), and the observed GBR degradation. Decades of continuing rise in atmospheric CO_2 with direct impact on rising sea surface temperatures that coral reefs must continually adapt to for survival give rise to a collective cause and effect memory. Putting atmospheric CO_2, sea surface temperatures, and GBR degradation in one unified stochastic framework gives us a better comparative scale and gauge of this interconnected collective ecological memory.

Components of an ecosystem may operate at different time scales, but they could reveal a behavioral imprint embedded in a collective memory of the rising atmospheric CO_2 that elevates sea surface temperatures leading to the GBR degradation. Extensive studies have shown a consistent heat gain by the earth system for the past decades. Energy, in the form of heat, leaving and entering the earth climate system is continually measured in terms of radiation at the top of the atmosphere (von Schuckmann 2020; Meyssignac et al 2019). Solar radiation heats the earth which in turn radiates back to space the reflected short wavelength radiation and longer wavelength infrared radiation (von Schuckmann et al 2020; Liu et al 2020; Meyssignac et al 2019). Re-emitted infrared from earth, however, is absorbed by atmospheric CO_2 and water vapor that cover the planet giving rise to a natural greenhouse effect. Hence, sunlight absorbed by earth is on average greater than outgoing longwave radiation (Carballo-Bolaños et al 2020; Meyssignac 2019; Anderson et al 2016). Greenhouse gases such as CO_2, which trap infrared radiation, have been continually increasing in the atmosphere due to fossil fuel combustion and other human activities (Hughes et al 2017; Hansen 2013; Yue and Gao 2018; Canadell et al 2007; Corti et al 1999). The energy accumulating in the climate system for decades has inevitably contributed to raised sea surface temperatures.

Using satellite and ocean data, a thorough study on how energy is accumulated and distributed within the climate system for the period 1985 – 2017 was recently done (Liu et al 2020). The biggest thermal reservoir on earth are the global oceans that cover most of the earth's surface with high heat capacity and absorbing more than 90% of earth's accumulated energy (Meyssignac

2019; Abraham et al 2013; Cheng et al 2017; Cheng et al 2019; von Schuckmann 2020). Since 1998, examined ocean basins have exhibited increased warming not only in the top ocean layer but also at deeper layers of the ocean with increasing ocean heat content (Cheng et al 2017; Liu et al 2020; Frade et al 2018; Schramek et al 2018) whose long-term effects could impact marine ecosystems such as the GBR, which stretches more than 2,300 km, being visible from outer space. The GBR has been losing more than 50% of its initial coral cover for the past decades (De'ath et al 2012; Mongin 2016; Hughes et al 2018; Hughes et al 2019).

Rising levels of atmospheric CO_2, in fact, poses a double threat to the GBR. Aside from elevated sea surface temperatures, ocean acidification also occurs when excess CO_2 in the atmosphere is absorbed by seawater. When CO_2 enters and dissolves in seawater, it produces a chemical reaction that yields H^+ ion concentration effectively lowering the pH of the ocean (Brown et al 2019; Albright et al. 2016; De'ath et al. 2012; Hughes et al. 2017; Mongin et al. 2016; Osborne 2017; Orr et al 2005; Anthony et al 2011). The GBR and levels of atmospheric CO_2, together with SST, constitute complex systems subjected to a number of intractable factors. The observables corresponding to these systems are characterized by fluctuations arising from short-term and long-term influences in time and in geographical location which may be periodic or non-periodic (Myers et al. 2018) exhibiting a collective ecological memory. The concern over the fate of the GBR has spurred various ways of modeling coral reef dynamics ranging from hydrodynamic models (Lambrechts et al. 2008; Mongin et al. 2016) to solving differential equations (Melbourne-Thomas et al. 2010; Wolanski et al. 2004), numerical models (Andutta et al. 2013; Zychaluk et al. 2012), and stochastic processes with varying assumptions (Andutta et al. 2013). Nonlinear correlations with past states may exist rendering Markovian modeling for time series data sets insufficient. Modeling fluctuating observables in the interrelated dynamics of the coral cover of the GBR, the rise in atmospheric CO_2 levels, and SST, therefore, finds a non-Markovian stochastic process most appropriate.

In climate models, introducing randomness or stochasticity is crucial in representing the many intractable unresolved factors that determine the fate of interconnected ecological systems. Stochasticity has been incorporated, for example, in the project Climate SPHINX (Stochastic Physics High Resolution Experiments) to predict future climate scenarios (Davini et al 2017; Meccia et al 2020; Strommen et al 2019; Yang et 2019). The inclusion of stochastic schemes into climate models has, for instance, improved global warming projections (Strommen et al 2019). Theoretically, there are many forms of stochastic processes with memory widely known as anomalous diffusion as exemplified by fractional Brownian motion (Metzler et al 2014; Biagini et al 2008; Mishura 2004; Sithi and Lim 1995). The stochastic process with memory used in this paper belongs to a larger class of non-Markovian white noise processes which have been successfully applied recently to investigate other systems such as the ageing of fibrin (Aure et al 2019), the DNA distribution in genomes (Violanda et al 2019), diffusion coefficient values for proteins of varying lengths (Barredo et al 2018), and cyclone track fluctuations (Bernido et al 2015), among others. We use an analytical stochastic framework with memory (Bernido and Carpio-Bernido 2012, 2015) which allows direct comparison between analytical and empirical results for the mean square deviation (MSD) of observables. Once the theoretical MSD has been matched with the empirically generated MSD of the fluctuating values

of the observables, we obtain an explicit analytical probability density function (PDF) describing the GBR degradation, as well as SST and atmospheric CO_2 levels. The PDF has a memory parameter μ and characteristic frequency ν with distinguishing values that define the memory behavior and comparative temporal evolution of the GBR degradation, elevated SST and atmospheric CO_2 levels.

The closed analytical expression for the PDF, which satisfies a modified diffusion equation with time-varying diffusion coefficient allows determination of various physical quantities of interest. An added insight into the temporal dynamics of the examined systems is obtained by looking at the short-time behavior of the time series data. Specifically, the fluctuating values of the dataset correspond theoretically to an anomalous diffusion where consecutive values are positively correlated. Short-time behavior of the analytical PDF and MSD reveals that SST and atmospheric CO_2 levels are characterized by fluctuating data point values in the superdiffusive regime, while the GBR degradation exhibits hyperballistic fluctuations.

2 Data and Methods

2.1 Observable Fluctuations in Empirical Datasets

We investigate three sets of empirical time series: (a) the mean percentage coral cover of the GBR from July 1985 to June 2011 obtained from the archives of the Australian Institute of Marine Science (AIMS) accessible through the data portal data.gov.au (AIMS, 2016); (b) Sea surface temperatures (https://www.ncdc.noaa.gov/teleconnections/enso/indicators/sst.php) from the climate monitoring division of NOAA for monthly data from January 1982 to October 2017; and (c) the Keeling curve for atmospheric CO_2 levels measured by the Mauna Loa Observatory of the National Oceanic Atmospheric Administration (NOAA, www.esrl.noaa.gov) in the island of Hawaii. Graphical representations for these three datasets are shown in Figures 1 to 3.

Figure 1 shows the mean percentage hard coral cover of the GBR from July 1985 to June 2011 obtained from the archives of the AIMS. Starting in the early 1980's, these data were gathered using manta tows to survey large areas of reefs and calculating the percentage of the perimeter of each reef that is covered with living and dead corals.

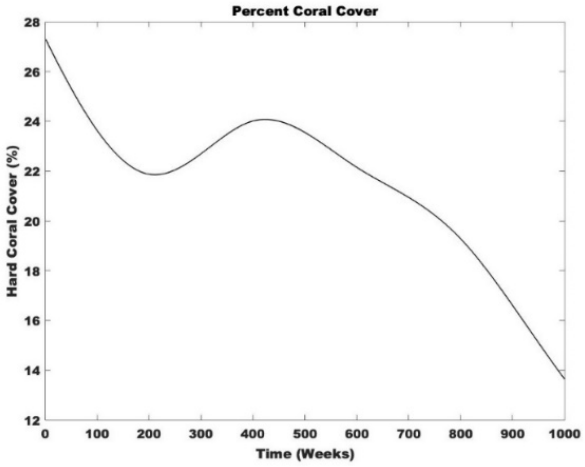

Figure 1. Percent of hard coral cover versus time (weeks) for the Great Barrier Reef (GBR).

For sea surface temperatures, there are four sets of data available depending on the region in the equatorial Pacific Ocean: Niño 1+2, Niño 3, Niño 3.4, and Niño 4. Specifically, we investigate the data closest to the Great Barrier Reef (18.2871° S, 147.6992° E) which is Niño 4 (5°N-5°S, 170°W-160°E) (https://www.ncdc.noaa.gov/teleconnections/enso/indicators/sst.php). The time series of SST is shown in Figure 2.

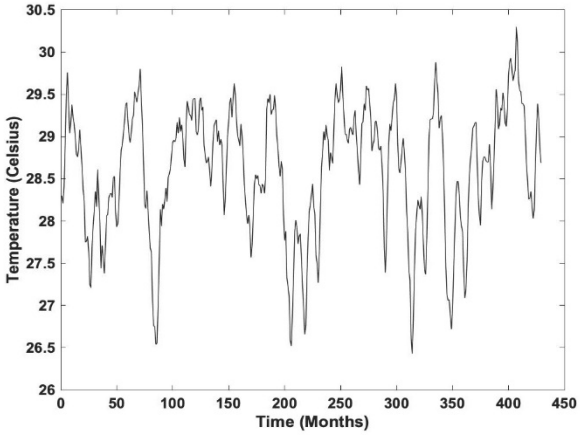

Figure 2. Sea surface temperatures at the equatorial Pacific Ocean (region: Niño 4).

Our study of the rising atmospheric CO_2 level, on the other hand, considers the Keeling curve for measurements taken since 1958 (www.esrl.noaa.gov) at the Mauna Loa Observatory. In particular, we take the weekly mean CO_2 data from May 1974 to August 2017, shown as open circles in Figure 3. Whereas fluctuation is quite straightforward for the GBR, and relatively random for sea surface temperatures (Figure 2), the atmospheric CO_2 levels exhibit a highly oscillatory data and certain periodicity. There are daily CO_2 level oscillations between night and day, as well as seasonal oscillations between Spring and Fall. For the weekly mean CO_2 levels from May 1974 to August 2017, we put a linear fit (solid line), or quadratic fit (dash-dot) for the empirical data (open circles) as shown in Figure 3.

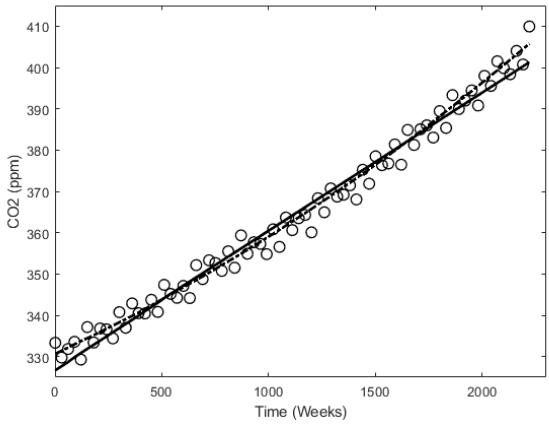

Figure 3. Atmospheric CO_2 levels. Empirical data (open circles) with a linear fit (solid line) and a quadratic fit (dash-dot).

One can plot fluctuations in the data of Figure 3 by subtracting each data point from the linear fit (solid line). Likewise, for comparison, we can do the same using the quadratic fit in Figure 3. The deviations from the linear and quadratic fits are shown in Figure 4.

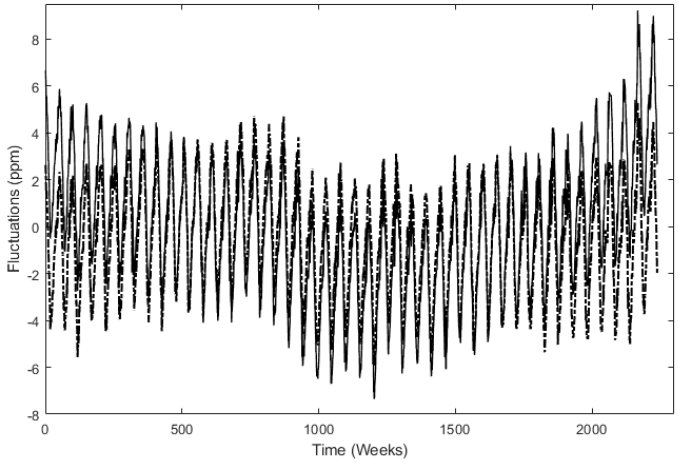

Figure 4. CO_2 fluctuations obtained by subtracting data points from the linear fit (solid line) and quadratic fit (dash-dot).

From the empirical data shown in Figures 1, 2, and 4, the mean square displacement (MSD) of the fluctuating observables are computed as a function of time. If the value of an observable is represented by $x(i)$ where i is a specific time, the MSD is computed as,

$$\mathrm{MSD}(\Delta t) = \frac{1}{N-\Delta t}\sum_{i=1}^{N-\Delta t}(x(i+\Delta t) - x(i))^2 \ , \tag{1}$$

with N the total number of data points. Here, $\Delta t < N$, is the time window, or lag time, which is an interval between two data points. Equation (1) gives an MSD value corresponding to a given Δt and to generate a MSD versus time plot, the Δt is increased up to a desired value. Note that as Δt increases, the number of sample deviations to be averaged in the dataset decreases. To avoid a lack of statistics, an upper limit for the value of Δt is imposed. This empirical MSD versus time plot could then be matched with a theoretical MSD of the stochastic analytical framework.

2.2 Stochastic Framework with Memory

The dataset we are using exhibits fluctuating values of the measured observables. Mathematically, we can capture the behavior of these fluctuations using a modulated Brownian motion $B(t)$. Designating a fluctuating variable as $x(t)$ which starts at x_0 at time, $t = 0$, and ends at, $t = T$, we can explicitly write, $x(t) = x_0 + fluctuations$, by parametrizing it as,

$$x(T) = x_0 + \int_0^T (T-t)^{(\mu-1)/2} t^{(\mu-1)/2} \sqrt{cos(\nu t)}\, dB(t). \tag{2}$$

In Eq. (2), the factor $(T-t)^{(\mu-1)/2}$ endows the system with memory as it evolves from time, $t = 0$, to a final time, $t = T = \pi/2\nu$. The memory behavior of the system changes depending on the value

of the memory parameter μ. On the other hand, the factor $t^{(\mu-1)/2}\sqrt{cos(\nu t)}$ in Eq. (2) modulates the Brownian motion $B(t)$ where ν is a characteristic frequency of the fluctuating measured observables. As shown in the Appendix, if we fix the endpoint of $x(t)$ to be at x_T at final time $t = T$, Eq. (2) leads to a probability density function (PDF) of the form (see Table 3.1, page 25, of Bernido and Carpio-Bernido 2015),

$$P(x_T, T; x_0, 0) = \left(\frac{\pi^{-\frac{3}{2}} T^{\frac{1}{2}-\mu} \nu^{\mu-\frac{1}{2}}}{2\,\Gamma(\mu) cos\left(\frac{\nu T}{2}\right) J_{\mu-\frac{1}{2}}\left(\frac{\nu T}{2}\right)} \right)^{\frac{1}{2}} exp\left\{ \frac{-T^{\frac{1}{2}-\mu} \nu^{\mu-\frac{1}{2}} (x_T - x_0)^2}{2\sqrt{\pi}\,\Gamma(\mu) cos\left(\frac{\nu T}{2}\right) J_{\mu-\frac{1}{2}}\left(\frac{\nu T}{2}\right)} \right\} . \tag{3}$$

In Eq. (3), $\Gamma(\mu)$ is the Gamma function and $J_\mu(z)$ is the Bessel function of the first kind. With this PDF one can also evaluate the mean square displacement (MSD) for $x(t)$, i.e., $\text{MSD} = \langle x^2 \rangle - \langle x \rangle^2$, where $\langle x^2 \rangle = \int_{-\infty}^{+\infty} x^2\, P(x, T; x_0, 0)\, dx$, with $P(x, T; x_0, 0)$ given by Eq. (3). This yields the result (Bernido and Carpio-Bernido 2015),

$$\text{MSD} = \frac{\Gamma(\mu) cos(\nu T/2)\, J_{\mu-\frac{1}{2}}(\nu T/2)}{\pi^{-\frac{1}{2}} T^{\frac{1}{2}-\mu} \nu^{\mu-\frac{1}{2}}} \quad . \tag{4}$$

The values for the parameters ν and μ would depend on the system being studied.

We observe that the probability density function, Eq. (3), can be written in the form,

$$P(x_T, T; x_0, 0) = \frac{1}{\sqrt{2\pi(\text{MSD})}} exp\left[\frac{-(x_T - x_0)^2}{2(\text{MSD})} \right] , \tag{5}$$

with a memory-dependent MSD, Eq. (4). This PDF gives us the flexibility of determining an initial and final point for the evolution of a system even for large times. Moreover, Eq. (5) obeys the modified diffusion equation (Barredo et al. 2018; Bernido and Carpio-Bernido 2015),

$$\frac{\partial P(x,t;x_0,0)}{\partial t} = \frac{1}{2}\left(\frac{\partial(\text{MSD})}{\partial t} \right) \frac{\partial^2 P(x,t;x_0,0)}{\partial x^2} \quad . \tag{6}$$

Equation (6) exhibits a time-dependent diffusion coefficient of the form, $\partial(\text{MSD})/\partial t$, which interestingly also occurs in other physical phenomena (Lee et al 2020; Reynaud 2017; Li et al 2018; Jeon et al 2014; Aure et al 2019; Barredo et al. 2018). We now proceed to apply this stochastic process with memory to acquire insights into the empirical datasets for the GBR degradation, sea surface temperatures near the GBR, and the rise of atmospheric CO_2 levels.

3 Results

3.1 Great Barrier Reef: Empirical and Theoretical Mean Square Displacements

To check whether the theoretical MSD, Eq. (4), indeed describes fluctuations for the percent of hard coral cover of the GBR, we let $\mu = 4.64$ and $\nu = 0.99$. Comparison of empirical and theoretical MSD is shown in Figure 5 where the solid line gives theoretical values and black dots for the empirical. The theoretical MSD generally captures the curve of the empirical MSD of the GBR.

Note that the theoretical MSD is normalized by multiplying it with a constant, i.e., N (MSD) where $N = 3.796$, and the time variable as T/T_C where $T_C = 0.910$. These normalizations of MSD and time T do not change the shape of the theoretical graph, Figure 5. The normalization N effectively raises the MSD graph with its shape unaltered, and T_C shifts the whole plot to the right so that empirical and theoretical plots are superimposed for easier comparison.

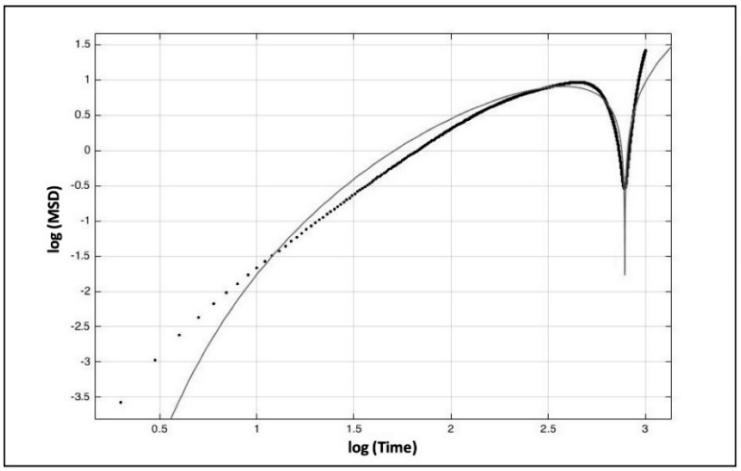

Figure 5. Great Barrier Reef percent hard coral cover empirical MSD (Black dots) using Eq. (1). Theoretical MSD (Solid line) using Eq. (4).

3.2 Sea Surface Temperatures: Empirical and Theoretical Mean Square Displacements

We now consider fluctuating values of sea surface temperatures shown in Figure 2. Evaluation of the mean square deviation yields an MSD shown in Figure 6.

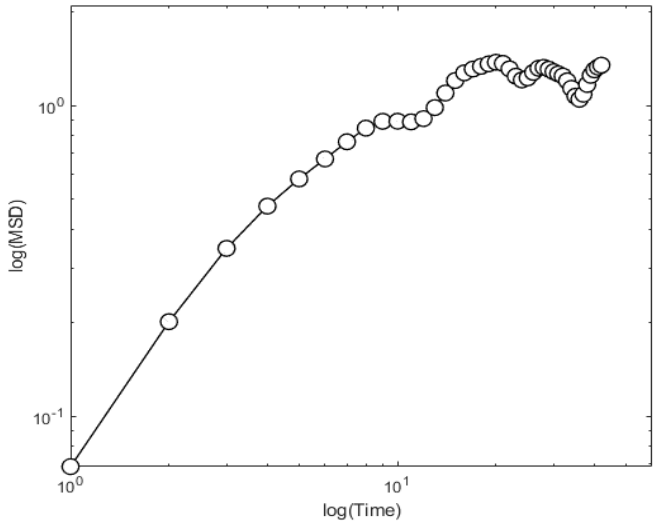

Figure 6. Empirical mean square deviations (MSD) using Eq. (1) for sea surface temperatures near the equatorial Pacific Ocean (region: Niño 4).

For SST, a match for the empirical MSD is obtained using the same stochastic behavior as the GBR degradation, i.e., Eqs. (2) to (4). In particular, empirical and theoretical MSD plots match for parameter values, $\mu = 1.18$ and $\nu = 0.19$, as shown in Figure 7. Again, for ease in comparing empirical and theoretical plots, we lower the analytical MSD graph without altering its shape using a normalization N (MSD), where $N = 0.11$.

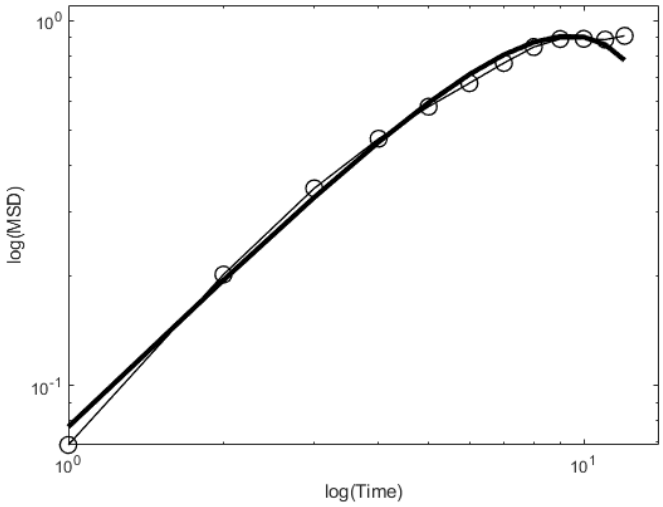

Figure 7. MSD for fluctuations in sea surface temperatures up to intervals of 12 months. Empirical (open circles); theoretical (thick solid line) using Eq. (4).

3.3 Atmospheric CO_2 Levels: Empirical and Theoretical Mean Square Displacements

Given the empirically derived fluctuations shown in Figure 4 for atmospheric CO_2 levels, one can plot the corresponding mean square displacements as shown in Figure 8.

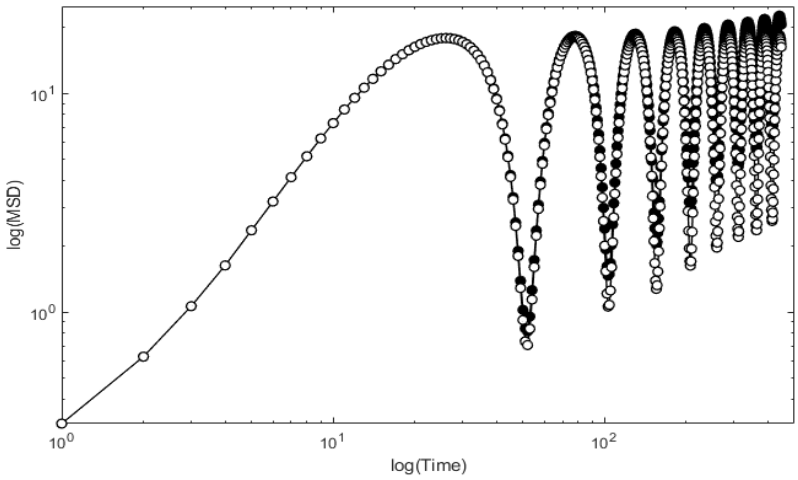

Figure 8. Empirical mean square deviations (MSD) using Eq. (1) for CO_2 fluctuations shown in Figure 4 for the quadratic fit (open circles) and linear fit (black circles).

The cyclic nature of atmospheric CO_2 levels clearly manifests in its log-log plot of MSD.

For CO_2 levels, empirical and theoretical MSD plots match for $\mu = 1.25$ and $\nu = 0.07$. For ease in comparing empirical and theoretical plots, we lower the analytical MSD graph without changing its shape with the normalization N (MSD), where $N = 0.4$. The comparison is shown in Figure 9.

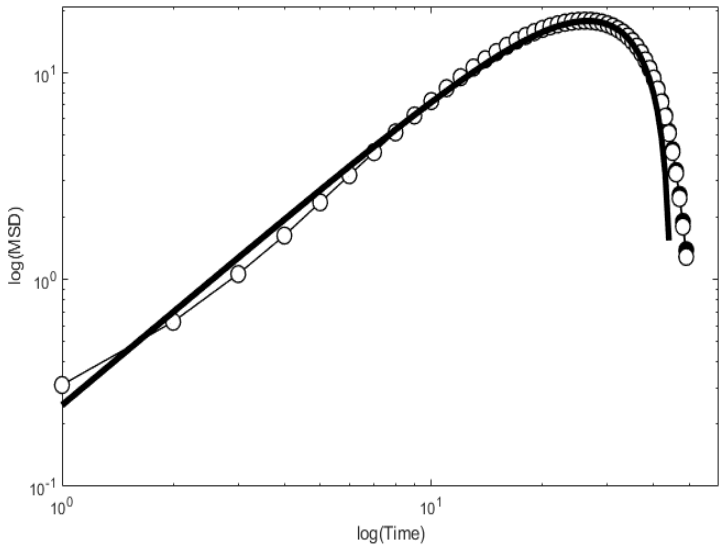

Figure 9. MSD for fluctuations in CO_2. Empirical (circles); theoretical (thick solid line) using Eq. (4).

4 Discussions

To help understand the similarities and interrelated dynamics of atmospheric CO_2 levels, SST, and declining hard coral cover of the GBR we used a stochastic process with memory as an analytical framework. A good match between empirical and theoretical MSD's was attained for each phenomenon indicating that all three systems are described by the same class of non-Markovian stochastic processes described by Eqs. (2) – (4). A comparative insight into the complex dynamics of the GBR degradation, SST, and atmospheric CO_2 levels can be seen by summarizing values of the memory parameter μ and characteristic frequency ν as shown in Table 1.

Table 1 Values for the memory parameter μ and characteristic frequency ν

SYSTEM	MEMORY PARAMETER μ	CHARACTERISTIC FREQUENCY ν
Great Barrier Reef (GBR) Degradation	$\mu = 4.64$	$\nu = 0.99$
CO_2 Levels	$\mu = 1.25$	$\nu = 0.07$
Sea Surface Temperatures (SST)	$\mu = 1.18$	$\nu = 0.19$

For both the memory parameter μ and characteristic frequency ν, the GBR degradation registers the highest values. Although the three systems are influenced by the same memory behavior of the form, $(T-t)^{(\mu-1)/2}$, the effect of the memory function differs with values of $\mu = 4.64$ for the GBR, $\mu = 1.25$ for CO_2 levels, and $\mu = 1.18$ for SST. Given the same values for an interval $(T-t)$, the impact of this memory range is greater for larger values of $\mu > 1$. Also, as seen in Eq. (2) the stochastic process loses its dependence on the memory function, $(T-t)^{(\mu-1)/2}$, at the critical value of $\mu = 1$.

For short-time intervals, all three systems exhibit a memory behavior different in form from Eqs. (2) to (4). Note that for $T \ll 1$, we can use the asymptotic forms, $cos(\nu T/2) \approx 1$, and $J_{\mu-(1/2)}(\nu T/2) \cong \left[1/\Gamma\left(\mu+(1/2)\right)\right](\nu T/4)^{\mu-(1/2)}$, which reduce Eq. (4) to a mean square deviation exhibiting a power law, i.e.,

$$\text{MSD} \approx c\, T^{\alpha}, \tag{7}$$

where, $\alpha = 2\mu - 1$, and $c = \sqrt{4\pi}\,\Gamma(\mu)/4^{\mu}\Gamma\left(\mu+(1/2)\right)$. The MSD, Eq. (7), is typical of anomalous diffusion with exponent α (Safdari et al 2017; Wang et al 2020; Metzler et al 2014). Table 1 gives us the values of the memory parameter μ which yield, $\alpha = 8.28$ for the GBR, $\alpha = 1.50$ for CO_2 levels, and $\alpha = 1.36$ for SST. The value of α has a physical implication on the behavior of the fluctuating values of the observables. In particular, $0 < \alpha < 1$, gives subdiffusive behavior whereas, $1 < \alpha < 2$, is superdiffusive (Metzler et al 2014; Biagini et al 2008). The case $\alpha = 2$ is the ballistic domain, while $2 < \alpha$ is referred to as hyperdiffusive or hyperballistic growth of the MSD that transpires, for example, in particle diffusion in turbulent flows or hyper-transport in optical systems (Safdari et al 2017; Wang et al 2020; Peccianti and Morandotti 2012; Levi et al 2012; Siegle et al 2010; Yao et al 1995). For, $1 < \alpha$, there is long range memory behavior where a fluctuating variable quickly departs from its point of origin as time evolves in comparison with ordinary Brownian motion. Given these values of the anomalous exponent α for $T \ll 1$, the fluctuating data points for CO_2 levels and SST belong to the superdiffusive regime, while the values for the GBR is hyperballistic in its growth of the MSD. Note that, although the short-time MSD, Eq. (7), is anomalous in nature, the stochastic process used here is Gaussian. This should be differentiated from the anomalous but non-Gaussian phenomenon which may involve, for example, the generalized grey Brownian motion (Ghosh et al 2016, Sposini 2018, Bock 2020).

We illustrate the different fluctuations or diffusion regimes in Figure 10 by plotting the probability density function with an MSD given by Eq. (7) for short-time intervals where the dashed line is subdiffusive ($\alpha < 1$), open boxes are superdiffusive ($1 < \alpha < 2$), and the solid line exemplifies hyperballistic diffusion ($2 < \alpha$). A subdiffusive fluctuation (dashed line; $\alpha = 0.4$) occurs when successive values of the data point x are negatively correlated resulting in larger possible values of $(x - x_0)$, where x_0 is an initial value. Superdiffusion (open boxes; $\alpha = 1.36$) has positively correlated consecutive values of x which result in lesser deviation in $(x - x_0)$ values when compared to subdiffusion. In a hyperballistic fluctuation (solid line; $\alpha = 2.3$), the values of $(x - x_0)$ are narrowly concentrated about the origin indicating that the value of x hardly fluctuates from an initial value x_0 as shown by its probability density function in Fig. 10. All plots in Fig. 10 were done at $T =$

0.2. Note that the critical value, $\alpha = 1$, or equivalently $\mu = 1$ in Eq. (2), corresponds to no memory or ordinary Brownian motion.

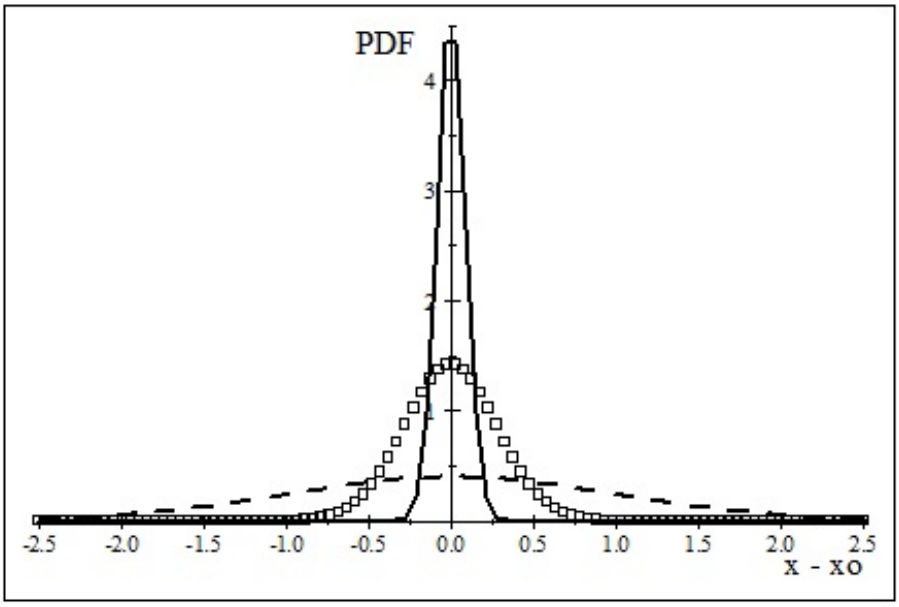

Figure 10. Probability density function for short-time intervals with MSD given by Eq. (7). Subdiffusion (dashed line, $\alpha = 0.4$); superdiffusion (open boxes, $\alpha = 1.36$); hyperballistic diffusion (solid line, $\alpha = 2.3$). All plots are at $T = 0.2$.

Figure 11 shows the MSD plots of Eq. (7) for anomalous diffusion ($\alpha = 1.5$ or $\mu = 1.25$) given by the straight red line, and ordinary Brownian motion for the case with no memory ($\alpha = 1$ or $\mu = 1$) as shown by the straight dashed line. For comparison, we also graph in Figure 11 the MSD, Eq. (4), for CO_2 levels with $\mu = 1.25$ and $\nu = 0.07$ which coincides with the anomalous diffusion for smaller values of *T*. Clearly, the memoryless Brownian motion (dashed line) and the power-law form of the MSD, Eq. (7), for anomalous diffusion (solid red line) are not able to capture the dip in MSD for longer times *T* exhibited by both the empirical MSD and theoretical MSD, Eq. (4), as shown for example in Figure 9. The MSD plots for the GBR, sea surface temperatures, and CO_2 levels given by Figures 5, 7, and 9, respectively, all experience a dip at longer time *T* which may imply a subdiffusive behavior. However, other intervening factors could allow its transition back to a superdiffusive regime. For possible oscillations between diffusion regimes, the GBR could be more prone to this given its high value for the characteristic frequency ν.

Figure 11. MSD for different memory behavior. Dashed line: Brownian motion (no memory); red straight line: anomalous diffusion; curved black line: stochastic process with memory describing the GBR, CO_2 levels, and sea surface temperatures.

The evolution in time for fluctuations corresponding to each phenomenon can be compared by plotting Eq. (3) for PDF versus time as illustrated in Figure 12. Here we set, $\Delta x = x_T - x_0 = 2$, in Eq. (3) and use the values for μ and ν in Table 1. Figure 12 shows that the PDF for all three phenomena reaches its peak roughly around the same time. The SST and atmospheric CO_2 levels essentially have the same probability distribution that appears to slowly diverge at longer times. The PDF of the GBR, however, drastically drops right after reaching its peak. This scenario implies that for a difference of 2 percent between initial and final hard coral cover, i.e., $\Delta x = 2$, the probability that this difference persists is close to zero after a certain time. On the other hand a difference in fluctuation of 2 ºC for SST and 2 ppm for CO_2 levels are possible and sustained even for longer times as depicted in Figure 12.

Figure 12. Probability density function (PDF) versus time for the GBR (black solid line, $\mu = 4.64$; $\nu = 0.99$), sea surface temperatures (circles, $\mu = 1.18$; $\nu = 0.19$), and CO_2 levels (dashed line, $\mu = 1.25$; $\nu = 0.07$).

5 Conclusion

The unified stochastic framework with memory gives us a snapshot through a common lens of three seemingly disparate but interrelated complex systems: the GBR, SST, and atmospheric CO_2. The inclusive framework allows for a comparison of the patterns exhibited by the datasets generated by each system. The translation of the behavior of datasets into an analytical stochastic setting shows that all three systems possess long term memory properties. Equation (7) tells us that for short-time intervals, $T \ll 1$, the datasets for all three systems reveal a mean square deviation of the measured observables growing in time as, $\text{MSD} \approx c\, T^{\alpha}$, where $\alpha = 2\mu - 1$, and c depends on the memory parameter μ (see Table 1). Each dataset examined exhibits anomalous diffusion where successive fluctuating values of measured observables are positively correlated. Specifically, for atmospheric CO_2 and SST, we have superdiffusive values of the exponent where, $1 < \alpha < 2$, while for the GBR degradation the value is, $2 < \alpha$, which falls in the hyperballistic domain. Stochastic acceleration or hyperballistic diffusion has been shown to result from a dynamically evolving disorder as demonstrated experimentally and numerically using an optical setting (Levi et al 2012). The lesser values of the anomalous exponent for atmospheric CO_2 ($\alpha = 1.50$) and SST ($\alpha = 1.36$), as compared to a large value of $\alpha = 8.28$ for the GBR, may be attributed to the fact that atmospheric CO_2 and the ocean are much larger systems than the GBR and, therefore, more capable of absorbing ecological disturbances. Their relative α values, however, quantify the observation that small fluctuations in atmospheric CO_2 and ocean temperatures could have a dramatic effect on the GBR. At finite times T, the MSD for the three systems transition to the full expression given by Eq. (4).

From the MSD, Eq. (4), characterized uniquely by the memory parameter μ and characteristic frequency ν for each system (Table 1), we also obtained an explicit form of the probability density function. The explicitly derived probability density functions and the modified diffusion equation, Eq. (6), for degradation of the Great Barrier Reef, sea surface temperatures, and atmospheric CO_2 levels provide a novel perspective and new insight on the temporal interrelated dynamics of these systems and a mathematical handle on effects of collective ecological memory.

Acknowledgments

The authors are grateful to Yutaka Shikano for his valuable comment. A. R. E. wishes to thank the Commission on Higher Education and C. B. C. the Department of Science and Technology for funding support. C. C. B. and M. V. C. B. acknowledge the support of PLDT-Smart Foundation.

Appendix: Deriving the probability density function

Consider a fluctuating variable $x(t)$ which starts at x_0 at time $t = 0$. Using the Brownian motion $B(t)$, we parametrize fluctuations up to some final time $t = T$ given by Eq. (2) as,

$$x(T) = x_0 + \int_0^T (T-t)^{(\mu-1)/2} t^{(\mu-1)/2} \sqrt{cos(\nu t)}\, dB(t) \quad , \tag{A1}$$

where, $(T-t)^{(\mu-1)/2}$, is a memory function, with $t^{(\mu-1)/2}\sqrt{cos(\nu t)}$ modulating ordinary Brownian motion $B(t)$. To evaluate the probability density function for this stochastic process, we express $dB(t)$ as $dB(t) = \omega(t)\, dt$, where $\omega(t)$ is the derivative of the Brownian motion (Hida et al. 1993), i.e., $\omega(t) = dB(t)/dt$. Note that, Eq. (A1) fixes the initial point at x_0 but the fluctuating variable can end anywhere at some final time $t = T$. We can fix the endpoint of $x(t)$ at time T to be, $x(T) = x_T$, using the Donsker delta function, $\delta(x(T) - x_T)$. This delta function is always zero for all paths described by Eq. (A1), except those which end at the chosen endpoint x_T. The expectation value for all contributing paths ending at x_T is an integral over the white noise variable $\omega(t)$,

$$P(x_T, T; x_0, 0) = \int \delta(x(T) - x_T)\; d\mu(\omega) \quad , \tag{A2}$$

where $d\mu(\omega)$ is the Gaussian white noise measure (Hida et al. 1993; Hida and Streit 2017; Kuo 1996; Obata 1994), and $P(x_T, T; x_0, 0)$ is the probability density function. To evaluate Eq. (A2), we write the Donsker delta function in terms of its Fourier representation, $\delta(x) = (1/2\pi)\int_{-\infty}^{+\infty} e^{ikx} dk$, to get,

$$P(x_T, T; x_0, 0) = \frac{1}{2\pi}\int_{-\infty}^{+\infty}\int exp\{ik[x(T) - x_T]\}\; dk\; d\mu(\omega). \tag{A3}$$

Using Eq. (A1) for $x(T)$ we have,

$$P(x_T, T; x_0, 0) = \frac{1}{2\pi}\int_{-\infty}^{+\infty} dk\; exp\{ik[x_0 - x_T]\}$$

$$\times \int exp\left\{ik\int_0^T (T-t)^{(\mu-1)/2} t^{(\mu-1)/2}\sqrt{cos(\nu t)}\;\omega(t)dt\right\}\; d\mu(\omega)\;. \tag{A4}$$

Integration over $d\mu(\omega)$ can be done using the characteristic functional (Hida et al. 1993),

$$\int exp\left\{i\int_0^T \omega(t)\varepsilon(t)dt\right\} d\mu(\omega) = exp\left[-\frac{1}{2}\int_0^T \varepsilon^2(t)\, dt\right], \tag{A5}$$

where we let, $\varepsilon(t) = k(T-t)^{(\mu-1)/2} t^{(\mu-1)/2}\sqrt{cos(\nu t)}$ in Eq. (A4). The key to making the model computable in the sense of explicitly evaluating expressions involving the Gaussian white noise variable $\omega(t)$ is the characteristic functional, Eq. (A5), which defines the Gaussian white noise measure $d\mu(\omega)$ (Hida et al. 1993; Hida and Streit 2017). Moreover, Eq. (A5) allows the generation of a wide class of stochastic processes with memory which has been applied to other biological and physical systems (Aure et al 2019; Violanda et al 2019; Barredo et al 2018; Bernido et al 2015). With Eq. (A5), the probability density function, Eq. (A4), becomes,

$$P(x_T, T; x_0, 0) = \frac{1}{2\pi}\int_{-\infty}^{+\infty} exp\{ik[x_0 - x_T]\}$$

$$\times exp\left\{-\frac{1}{2}k^2\int_0^T \left[(T-t)^{(\mu-1)/2} t^{(\mu-1)/2}\sqrt{cos(\nu t)}\right]^2 dt\right\} dk. \tag{A6}$$

The remaining integral over *dk* is a Gaussian integral which yields the probability density function (Bernido and Carpio-Bernido 2015),

$$P(x_T, T; x_0, 0) = \frac{1}{\sqrt{2\pi \int_0^T (T-t)^{\mu-1} t^{\mu-1} cos(\nu t) dt}} exp\left[\frac{-(x_T - x_0)^2}{2\int_0^T (T-t)^{\mu-1} t^{\mu-1} cos(\nu t) dt}\right]. \qquad \text{(A7)}$$

We then obtain Eq. (3) using Eq. (3.768.9) of Gradshteyn and Ryzhik (1994) to integrate over *dt* in Eq. (A7).

DECLARATIONS:

The authors have no conflicts of interest to declare that are relevant to the content of this article.

REFERENCES

Abraham JP, Baringer M, Bindoff NL, Boyer T, Cheng LJ, Church JA, Conroy JL, Domingues CM, Fasullo JT, Gilson J, Goni G, Good SA, Gorman JM, Gouretski V, Ishii M, Johnson GC, Kizu S, Lyman JM, Macdonald AM, and Willis JK (2013) A review of global ocean temperature observations: Implications for ocean heat content estimates and climate change, Rev. Geophys., **51**: 450–483, https://doi.org/10.1002/rog.20022.

Albright R, Caldeira L, Hosfelt J, et al (2016) Reversal of ocean acidification enhances net coral reef calcification. Nature **531**: 362-365.

Anderson TR, Hawkins E, Jones PD (2016) CO2, the greenhouse effect and global warming: from the pioneering work of Arrhenius and Callendar to today's Earth System Models. Endeav. **40**: 178-187.

Andutta FP, Ridd PV, and Wolanski E (2013) The age and the flushing time of the Great Barrier Reef waters. Continental Shelf Res. **53**: 11-19.

Anthony KRN, Maynard JA, Diaz-Pulido G, Mumby PJ, Marshall PA, Cao L, and Hoegh-Guldberg O (2011) Ocean acidification and warming will lower coral reef resilience. Glob. Change Biol. **17**: 1798-1808; doi: 10.1111/j.1365-2486.2010.02364.x.

Aure RRL, Bernido CC, Carpio-Bernido MV, and Bacabac RG (2019) Damped white noise diffusion with memory for diffusing microprobes in ageing fibrin gels, Biophys. Jour. **117**: 1029–1036.

Barredo W, Bernido CC, Carpio-Bernido MV, and Bornales JB (2018) Modelling non-Markovian fluctuations in intracellular biomolecular transport. Math. Biosci. **297**: 27-31.

Bernido CC and Carpio-Bernido MV (2012) White noise analysis: some applications in complex systems, biophysics and quantum mechanics. Int. J. Mod. Phys. B **26**: 1230014.

Bernido CC and Carpio-Bernido MV (2015) Methods and Applications of White Noise Analysis in Interdisciplinary Sciences. World Scientific, Singapore.

Bernido CC, Carpio-Bernido MV, Escobido MGO (2014), Modified diffusion with memory for cyclone track fluctuations, Phys. Lett. A **378**: 2016-2019; (2015) **379**: 230-231.

Biagini F, Hu Y, Øksendal B, Zhang T (2008) Stochastic Calculus for Fractional Brownian Motion and Applications. Springer-Verlag, London.

Bock W, Desmettre S, and da Silva JL (2020) Integral representation of generalized grey Brownian motion. Stochastics **92**: 552-565. DOI: 10.1080/17442508.2019.1641093.

Brown BE, Dunne RP, Edwards AJ, Sweet MJ, and Phongsuwan N (2015) Decadal environmental 'memory' in a reef coral? Mar. Biol. **162:** 479–483. DOI 10.1007/s00227-014-2596-2.

Brown BE, Dunne RP, Somerfeld PJ, Edwards AJ, Simons WJF, Phongsuwan N, Putchim L, Anderson L, and Naeije MC (2019) Long-term impacts of rising sea temperature and sea level on shallow water coral communities over a ~40 year period. Sci. Rep. **9**:8826 | https://doi.org/10.1038/s41598-019-45188-x.

Canadell JG, Quéré CL, Raupach MR, Field CB, Buitenhuis ET et al (2007) Contributions to accelerating atmospheric CO_2 growth from economic activity, carbon intensity, and efficiency of natural sinks. Proc. Natl. Acad. Sci. USA **104** :18866–18870.

Carballo-Bolaños R, Soto D, and Chen CA (2020) Thermal stress and resilience of corals in a climate-changing world. J. Mar. Sci. Eng. **8**:15. doi:10.3390/jmse8010015.

Cheng L, Abraham J, Hausfather Z, and Trenberth KE (2019). How fast are the oceans warming? Science **363**: 128–129. https:// doi.org/10.1126/science.aav7619

Cheng L, Trenberth KE, Fasullo J, Boyer T, Abraham J, Zhu J (2017) Improved estimates of ocean heat content from 1960 to 2015. Sci. Adv. **3**: e1601545. https://doi.org/10.1126/sciadv.1601545.

Corti S, Molteni F, and Palmer T (1999) Signature of recent climate change in frequencies of natural atmospheric circulation regimes. Nature **398**: 799–802. https://doi.org/10.1038/19745.

Corti S, Weisheimer A, Palmer TN, Doblas-Reyes FJ, and Magnusson L (2012) Reliability of decadal predictions. Geophys. Res. Lett. **39**: L21712, doi:10.1029/2012GL053354.

Davidson J, Thompson A, Logan M, Schaffelke B (2019) High spatio-temporal variability in Acroporidae settlement to inshore reefs of the Great Barrier Reef. PLoS ONE **14**: e0209771. https://doi.org/10.1371/journal. pone.0209771.

Davini P, von Hardenberg J, Corti S et al (2017). Climate SPHINX: evaluating the impact of resolution and stochastic physics parameterisations in the EC-Earth global climate model. Geosci. Model Dev. **10**: 1383–1402. www.geosci-model-dev.net/10/1383/2017/ doi:10.5194/gmd-10-1383-2017.

De'ath G, Fabricius KE, Sweatman H, and Puotinen M (2012) The 27-year decline of coral cover on the Great Barrier Reef and its causes. Proceedings of the National Academy of Sciences of USA **109** (44):17995-17999.

Fine M, Hoegh-Guldberg O, Meroz-Fine E et al. (2019) Ecological changes over 90 years at Low Isles on the Great Barrier Reef. Nat Commun **10**: 4409. https://doi.org/10.1038/s41467-019-12431-y.

Frade PR et al. (2018) Deep reefs of the Great Barrier Reef offer limited thermal refuge during mass coral bleaching. Nat. Commun. **9**: 3447.

Ghosh SK, Cherstvy AG, Grebenkov DS, and Metzler R (2016) Anomalous, non-Gaussian tracer diffusion in crowded two-dimensional environments. *New J. Phys.* **18**: 013027.

Gradshteyn IS and Ryzhik IM (1994) Table of Integrals, Series and Products, 5th edition. Academic Press, San Diego.

Hansen J, Sato M, Russell G, and Kharecha P (2013) Climate sensitivity, sea level and atmospheric carbon dioxide. Phil. Trans. R. Soc. A **371**: 20120294. http://dx.doi.org/10.1098/rsta.2012.0294.

Hida T, Kuo HH, Potthoff J, Streit L (1993) White Noise - An Infinite Dimensional Calculus. Kluwer, Dordrecht.

Hida T and Streit L (2017) Let Us Use White Noise. World Scientific, Singapore.

Hughes T, Barnes M, Bellwood D et al. (2017) Coral reefs in the Anthropocene. Nature **546**: 82–90. https://doi.org/10.1038/nature22901.

Hughes TP, Kerry JT, Álvarez-Noriega M, Álvarez-Romero JG, Anderson KD, Baird AH, Babcock RC, Beger M, Bellwood DR, Berkelmans R, Bridge TC, Butler IR, Byrne M, Cantin NE, Comeau S, Connolly SR, Cumming GS, Dalton SJ, Diaz-Pulido G, Eakin CM, Figueira WF, Gilmour JP, Harrison HB, Heron SF, Hoey AS et al (2017) Global warming and recurrent mass bleaching of corals. Nature **543**:373-377.

Hughes et al (2019) Ecological memory modifies the cumulative impact of recurrent climate extremes. Nature Clim. Change **9**: 40–43.

Jeon J-H, Chechkin AV, and Metzler R (2014) Scaled Brownian motion: a paradoxical process with a time dependent diffusivity for the description of anomalous diffusion. Phys. Chem. Chem. Phys. **16**: 15811.

Johnstone JF et al (2016) Changing disturbance regimes, ecological memory, and forest resilience. Front. Ecol. Environ. **14**: 369–378.

Jurriaans S, Hoogenboom MO. (2019) Thermal performance of scleractinian corals along a latitudinal gradient on the Great Barrier Reef. Phil. Trans. R. Soc. B **374**: 20180546. http://dx.doi.org/10.1098/rstb.2018.0546

Kuo HH (1996) White Noise Distribution Theory (CRC, Boca Raton).

Lambrechts J, Hanert E, Deleersnijder E, Bernard P-E, Legat V, Remacle J-F, and Wolanski E (2008) A multi-scale model of the hydrodynamics of the whole Great Barrier Reef. Estuarine, Coastal and Shelf Science **79**:143-151.

Lee HH, Papaioannou A, Kim SL et al. (2020) A time-dependent diffusion MRI signature of axon caliber variations and beading. Commun Biol **3**: 354. https://doi.org/10.1038/s42003-020-1050-x

Levi L, Krivolapov Y, Fishman S, and Segev M (2012) Hyper-transport of light and stochastic acceleration by evolving disorder. Nature Phys **8**: 912–917. https://doi.org/10.1038/nphys2463.

Li C-W, Xue H-L, Guan C, and Liu W-b (2018) Modeling and experiments for the time-dependent diffusion coefficient during methane desorption from coal, Jour. Geophys. and Engineer **15**: 315–329. https://doi.org/10.1088/1742-2140/aa98ba

Liu C, Allan RP, Mayer M, Hyder P, Desbruyères D, Cheng L, Xu J, Xu F, Zhang Y (2020) Variability in the global energy budget and transports 1985–2017. Clim Dyn **55**:3381–3396.

Meccia VL, Fabiano F, Davini P, and Corti S (2020). Stochastic parameterizations and the climate response to external forcing: An experiment with EC-Earth. Geophys. Res. Lett. **47**: e2019GL085951. https://doi.org/10.1029/2019GL085951.

Melbourne-Thomas J, Johnson CR, Aliño PM, Geronimo RC, Villaloy CL and Gurney GG (2010) A multi-scale biophysical model to inform regional management of coral reefs in the western Philippines and South China Sea. Environ. Model. Software, **26**:66–82.

Metzler R, Jeon J-H, Cherstvy AG, and Barkai E (2014) Anomalous diffusion models and their properties: non-stationarity, non-ergodicity, and ageing at the centenary of single particle tracking. Phys. Chem. Chem. Phys. **16**: 24128.

Meyssignac B, Boyer T, Zhao Z, Hakuba MZ, Landerer FW et al (2019) Measuring global ocean heat content to estimate the earth energy imbalance. Front. Mar. Sci. **6** : 432. https://doi.org/10.3389/fmars.2019.00432

Mishura Y (2008) Stochastic Calculus for a Fractional Brownian Motion and Related Processes. Springer-Verlag, Berlin.

Mongin M, Baird ME, Tilbrook B, Matear RJ, Lenton A, Herzfeld M, Wild-Allen K, Skerratt J, Margvelashvili N, Robson BJ, Duarte CM, Gustafsson MSM, Ralph PJ and Steven ADL (2016) The exposure of the Great Barrier Reef to ocean acidification. Nat. Commun. **7**:10732 doi: 10.1038/ncomms10732.

Mumby PJ and van Woesik R (2014) Consequences of ecological, evolutionary and biogeochemical uncertainty for coral reef responses to climatic stress. Curr. Biol. **24**: R413-R423.

Myers TA, Mechoso CR, DeFlorio MJ (2018) Coupling between marine boundary layer clouds and summer-to-summer sea surface temperature variability over the North Atlantic and Pacific. Clim. Dyn. **50**:955-969.

Nyström M and Folke C (2001) Spatial resilience of coral reefs. Ecosyst. **4**: 406-417.

Obata N (1994) White Noise Calculus and Fock Space. Lecture Notes in Mathematics, Vol. 1577 (Springer, Berlin).

Ogle K. et al (2015) Quantifying ecological memory in plant and ecosystem processes. Ecol. Lett. **18**: 221–235.

Orr JC et al (2005) Anthropogenic ocean acidification over the twenty-first century and its impact on calcifying organisms. Nature **437**: 681-686.

Osborne K, Thompson AA, Cheal AJ, et al (2017) Delayed coral recovery in a warming ocean. Glob. Change Biol. 1–13. https://doi.org/10.1111/ gcb.13707.

Payne MR et al (2017) Lessons from the first generation of marine ecological forecast products. Front. Mar. Sci. **4**:289. https://doi.org/10.3389/fmars.2017.00289.

Peccianti M., Morandotti R (2012) Beyond ballistic. Nature Phys **8**: 858–859. https://doi.org/10.1038/nphys2486.

Peterson GD (2002) Contagious disturbance, ecological memory, and the emergence of landscape pattern. Ecosyst. **5**: 329–338. https://doi.org/10.1007/s10021-001-0077-1.

Reynaud O (2017) Time-dependent diffusion MRI in cancer: tissue modeling and applications. Front. Phys. **5**: 58. https://doi.org/10.3389/fphy.2017.00058.

Romero-Torres M, Acosta A, Palacio-Castro AM, et al. (2020) Coral reef resilience to thermal stress in the Eastern Tropical Pacific. Glob Change Biol. **26**:3880–3890. https://doi.org/10.1111/gcb.15126.

Safdari H, Cherstvy AG, Chechkin AV, Bodrova A, and Metzler R (2017) Aging underdamped scaled Brownian motion: Ensemble- and time-averaged particle displacements, nonergodicity, and the failure of the overdamping approximation. Phys. Rev. E **95**: 012120.

Schramek TA, Colin PL, Merrifield MA, and Terrill EJ (2018) Depth-dependent thermal stress around corals in the tropical Pacific Ocean. Geophys. Res. Lett. **45**:9739–9747.

Schweiger AH, Boulangeat I, Conradi T, Davis M, and Svenning J-C (2018) The importance of ecological memory for trophic rewilding as an ecosystem restoration approach. Biol. Rev. 000–000. 1 doi: 10.1111/brv.12432.

Siegle P, Goychuk I, and Hänggi P (2010) Origin of hyperdiffusion in generalized Brownian motion. Phys. Rev. Lett. **105**: 100602.

Sithi VM and Lim SC (1995) On the spectra of Riemann-Liouville fractional Brownian motion. J. Phys. A: Math. Gen. **28**: 2995-3003.

Sposini V, Chechkin AV, Seno F, Pagnini G, and Metzler R (2018) Random diffusivity from stochastic equations: comparison of two models for Brownian yet non-Gaussian diffusion. New J. Phys. **20**: 043044.

Strommen K, Watson PAG, and Palmer TN (2019). The impact of a stochastic parameterization scheme on climate sensitivity in EC-Earth. Jour. Geophys. Res.: Atmos. **124**: 12,726–12,740. https://doi.org/10.1029/2019JD030732

Sully S, Burkepile DE, Donovan MK, Hodgson G and van Woesik R (2019) A global analysis of coral bleaching over the past two decades. Nat Commun **10,** 1264 (2019). https://doi.org/10.1038/s41467-019-09238-2.

Thomas L and Palumbi SR (2017) The genomics of recovery from coral bleaching. Proc. R. Soc. B **284**: 20171790. http://dx.doi.org/10.1098/rspb.2017.1790.

Turner MG et al. (2020) Climate change, ecosystems and abrupt change: science priorities. Phil. Trans. R. Soc. B **375**: 20190105. http://dx.doi.org/10.1098/rstb.2019.0105.

van der Bolt B, van Nes EH, Bathiany S, Vollebregt ME and Scheffer M (2018) Climate reddening increases the chance of critical transitions. Nature Clim. Change **8**: 478–484.

von Schuckmann K et al (2020) Heat stored in the Earth system: where does the energy go? Earth Syst Sci Data **12**:2013–2041.

Violanda RR, Bernido CC, and Carpio-Bernido MV (2019) White noise functional integral for exponentially decaying memory: nucleotide distribution in bacterial genomes, Phys. Scr. **94**: 125006.

Wang W, Cherstvy AG, Liu X, and Metzler R (2020) Anomalous diffusion and nonergodicity for heterogeneous diffusion processes with fractional Gaussian noise. Phys. Rev. E **102**: 012146

Wolanski E, Richmond RH, and McCook L (2004) A model of the effects of land-based, human activities on the health of coral reefs in the Great Barrier Reef and in Fouha Bay, Guam, Micronesia. J. Mar. Syst. **46**:133–144.

Yang C, Christensen HM, Corti S et al. (2019) The impact of stochastic physics on the El Niño Southern Oscillation in the EC-Earth coupled model. Clim Dyn **53**: 2843–2859. https://doi.org/10.1007/s00382-019-04660-0.

Yao HB, Zabusky NJ, Dritschel DG (1995) High gradient phenomena in two-dimensional vortex interactions. Phys. Fluids **7**: 539-548.

Yuan N, Huang Y, Duan J, Zhu C, Xoplaki E, and Luterbacher J (2019) On climate prediction: how much can we expect from climate memory. Clim. Dyn. **52**:855–864. https://doi.org/10.1007/s00382-018-4168-5.

Yue X-L and Gao Q-X (2018) Contributions of natural systems and human activity to greenhouse gas emissions. Adv. Clim. Change Res. **9**: 243-252.

Zychaluk K, Bruno JF, Clancy D, McClanahan TR and Spencer M (2012) Data-driven models for regional coral-reef dynamics. Ecol. Lett. **15**:151-158.

Figures

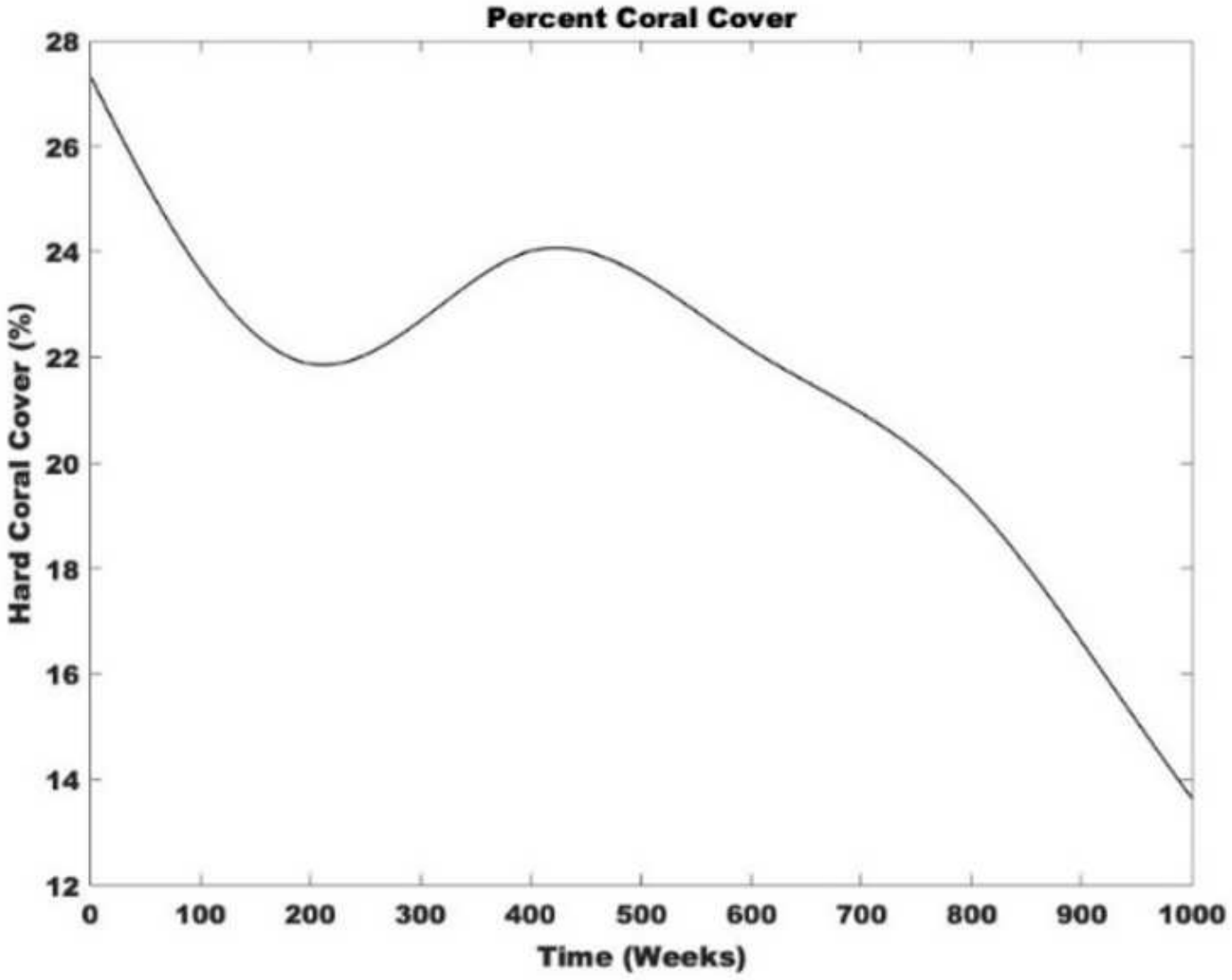

Figure 1

Percent of hard coral cover versus time (weeks) for the Great Barrier Reef (GBR).

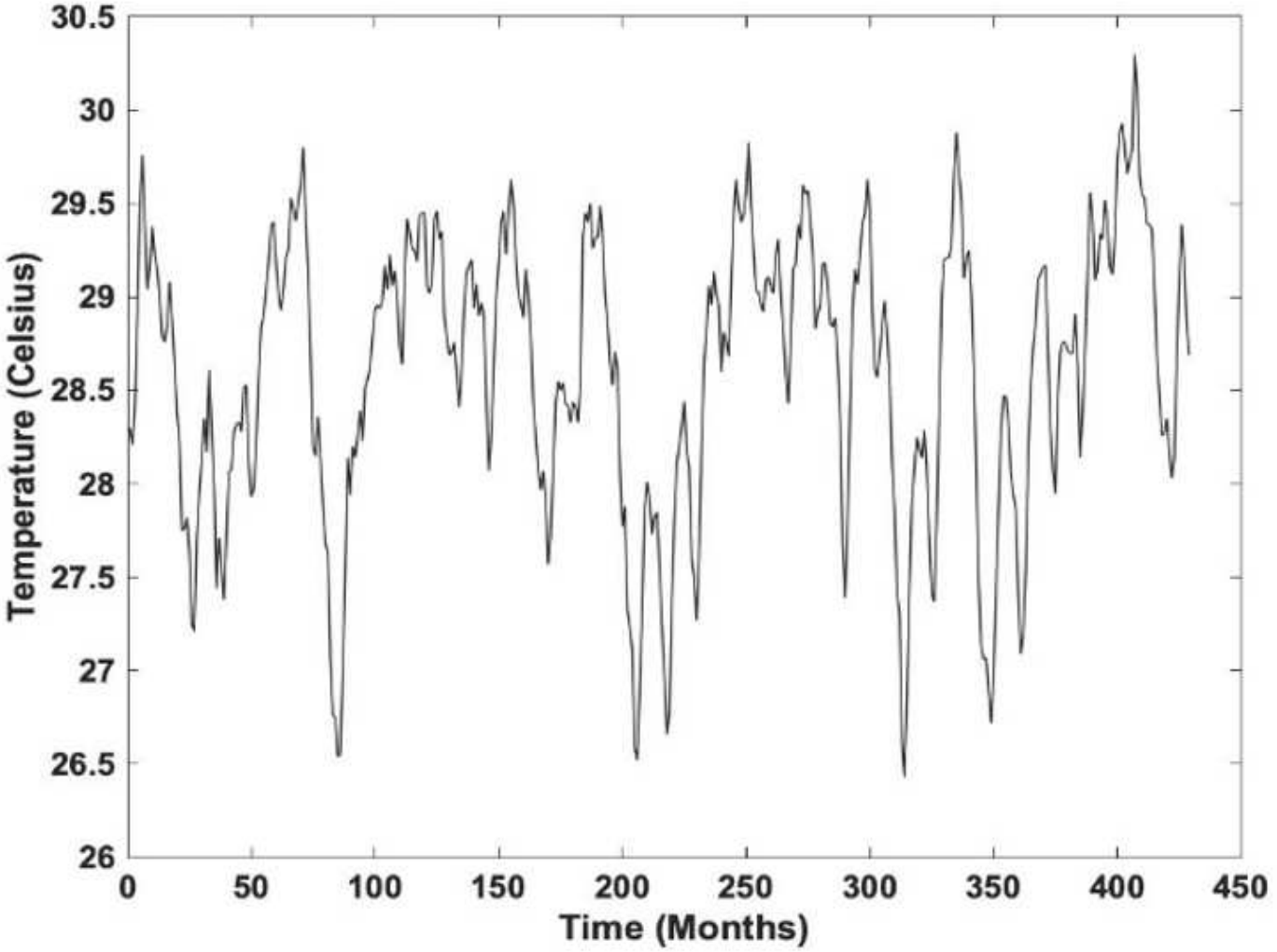

Figure 2

Sea surface temperatures at the equatorial Pacific Ocean (region: Niño 4).

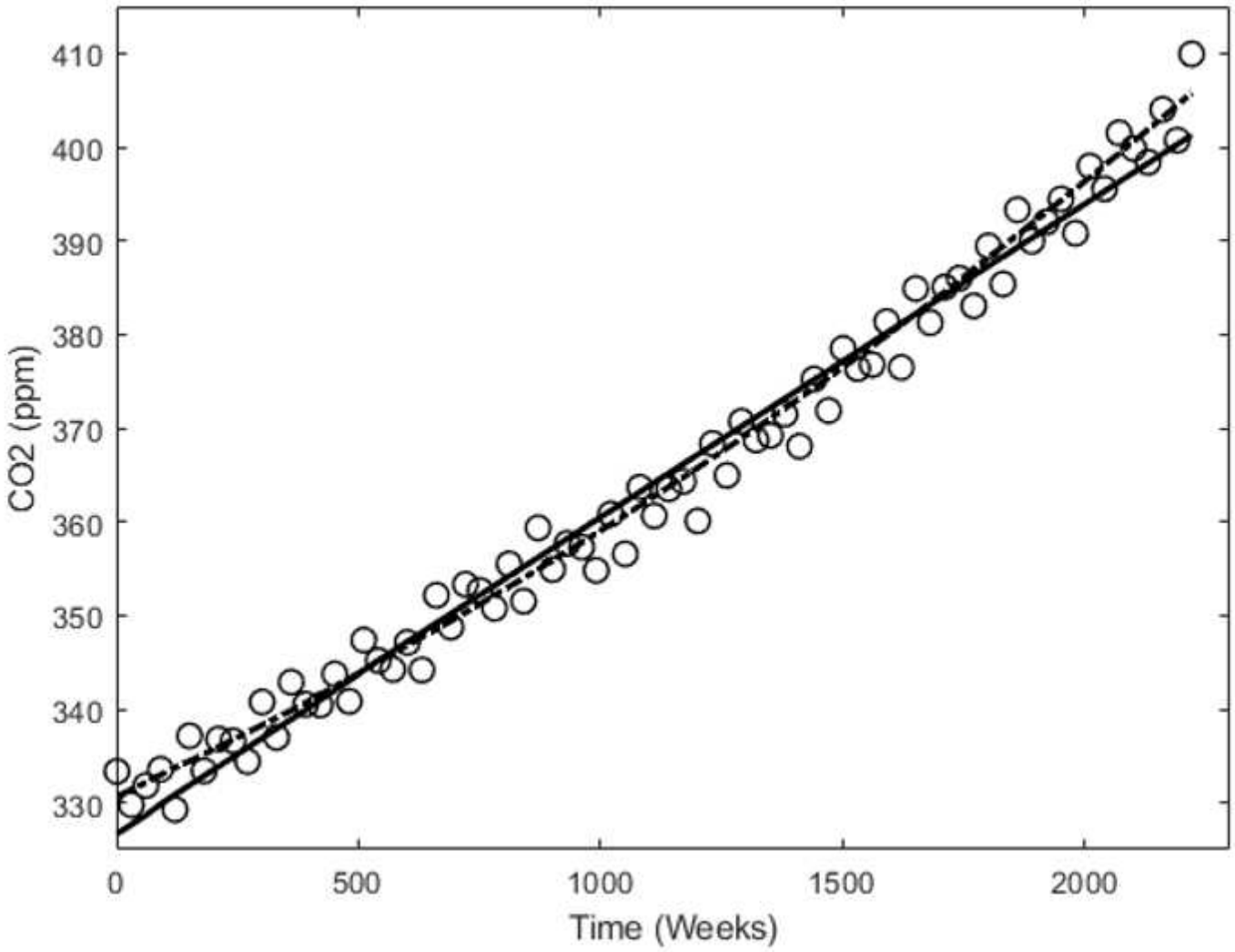

Figure 3

Atmospheric CO2 levels. Empirical data (open circles) with a linear fit (solid line) and a quadratic fit (dash-dot).

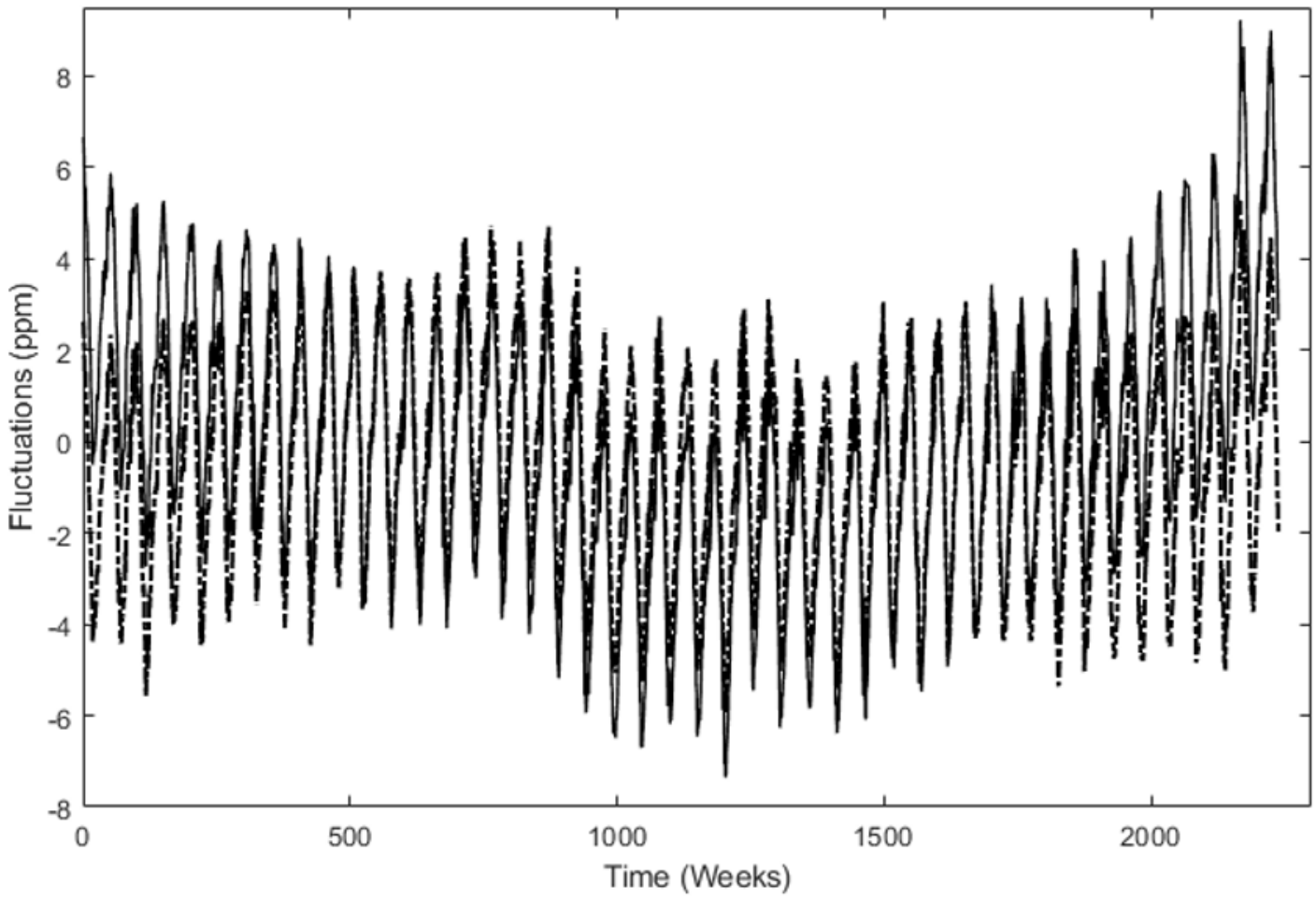

Figure 4

CO2 fluctuations obtained by subtracting data points from the linear fit (solid line) and quadratic fit (dash-dot).

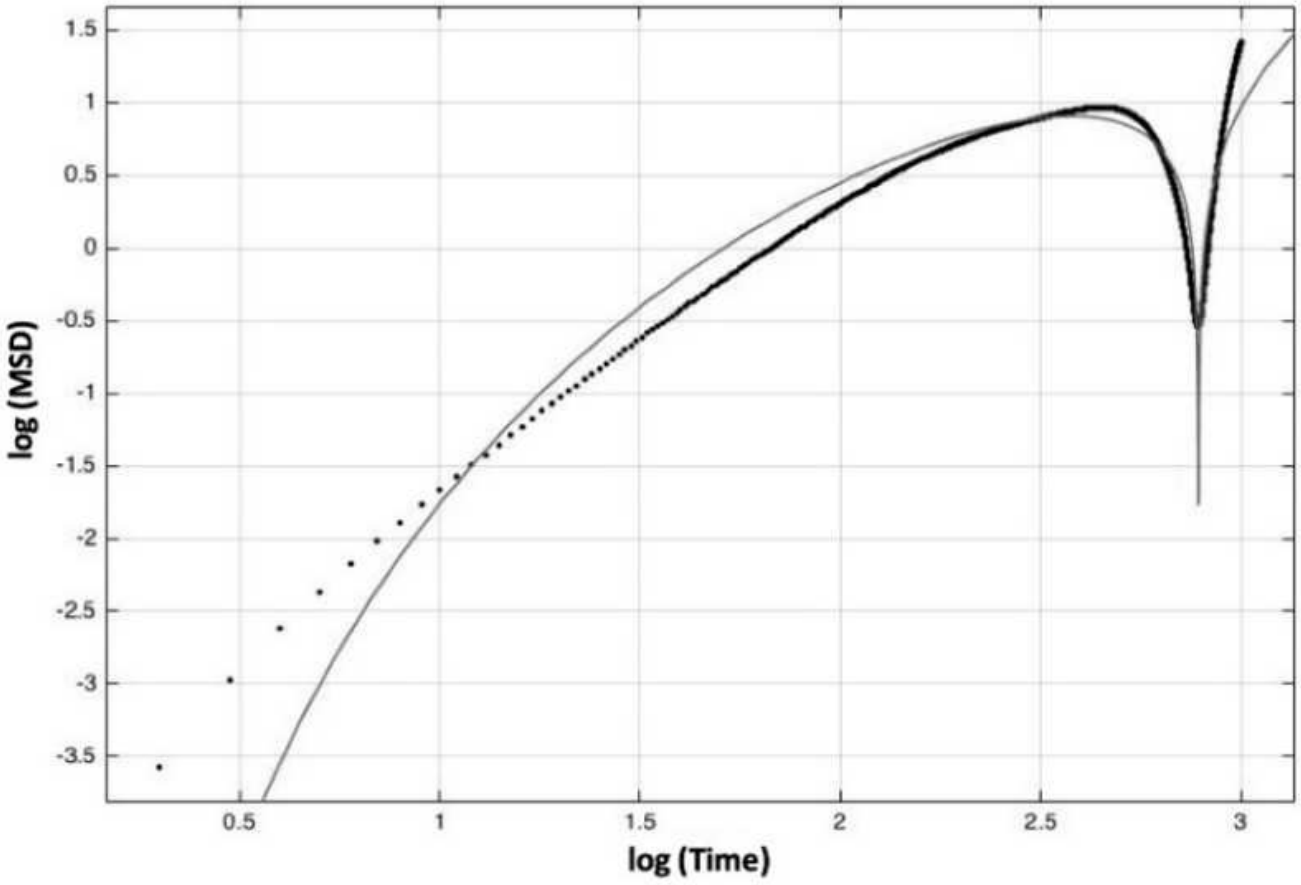

Figure 5

Great Barrier Reef percent hard coral cover empirical MSD (Black dots) using Eq. (1). Theoretical MSD (Solid line) using Eq. (4).

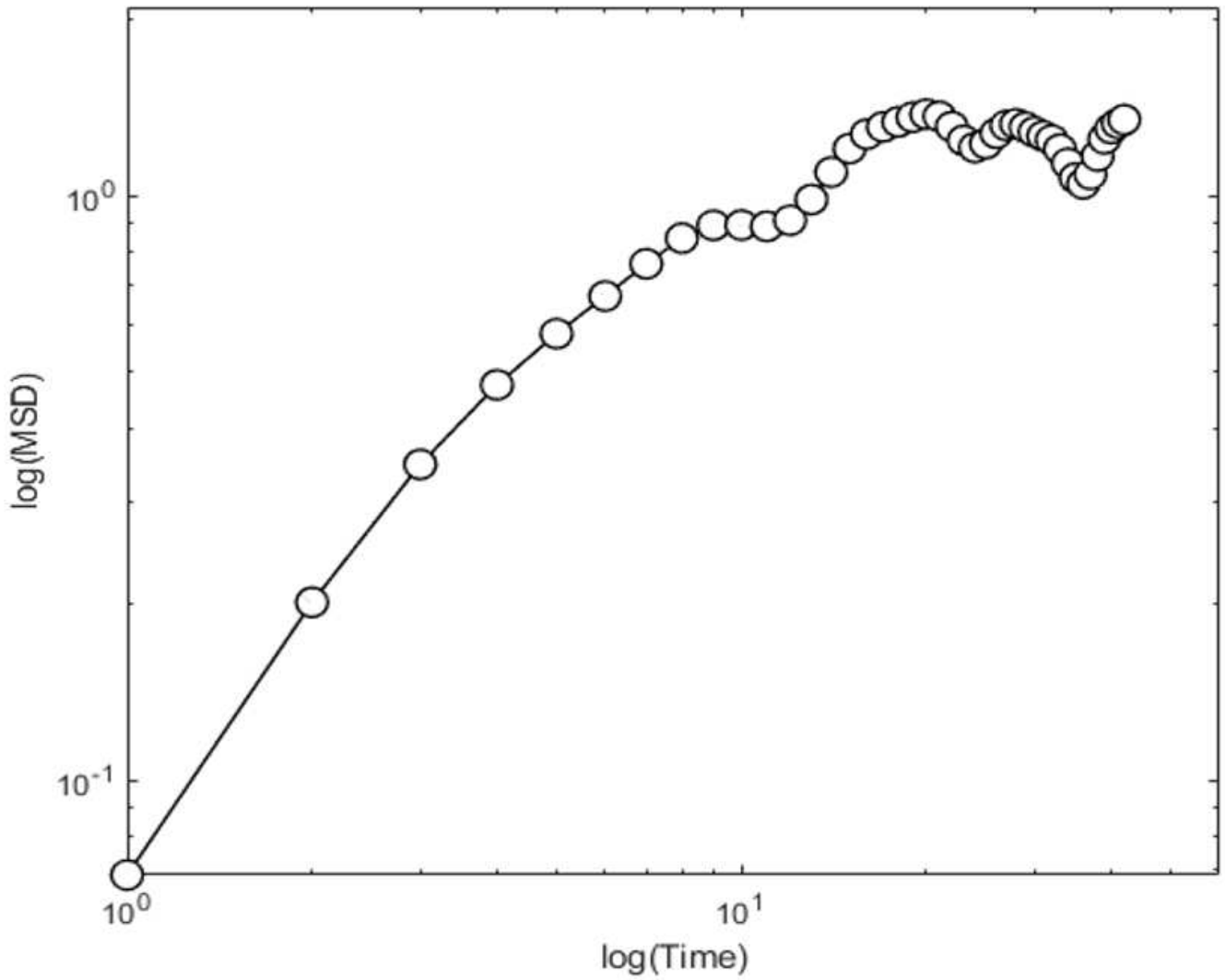

Figure 6

Empirical mean square deviations (MSD) using Eq. (1) for sea surface temperatures near the equatorial Pacific Ocean (region: Niño 4).

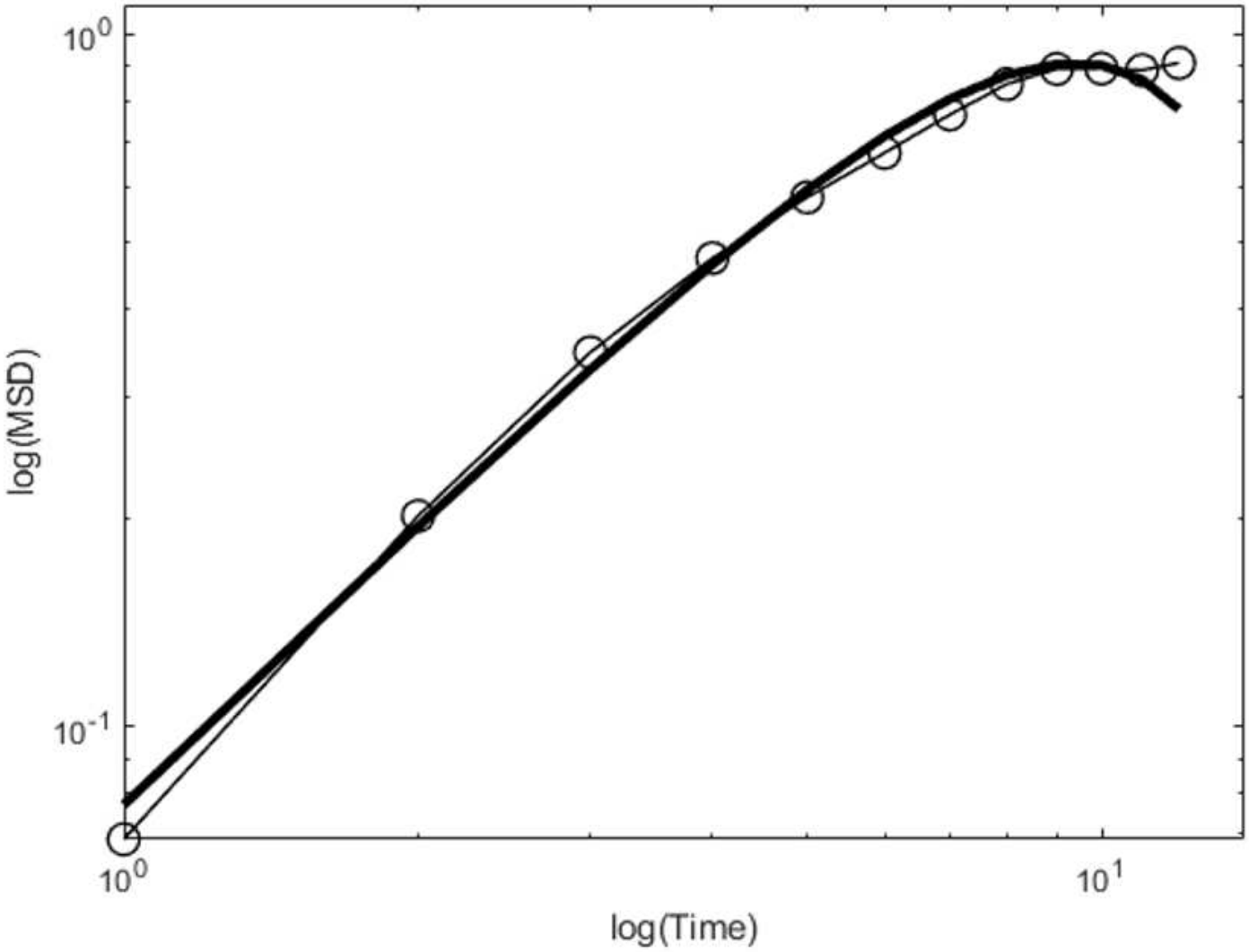

Figure 7

MSD for fluctuations in sea surface temperatures up to intervals of 12 months. Empirical (open circles); theoretical (thick solid line) using Eq. (4).

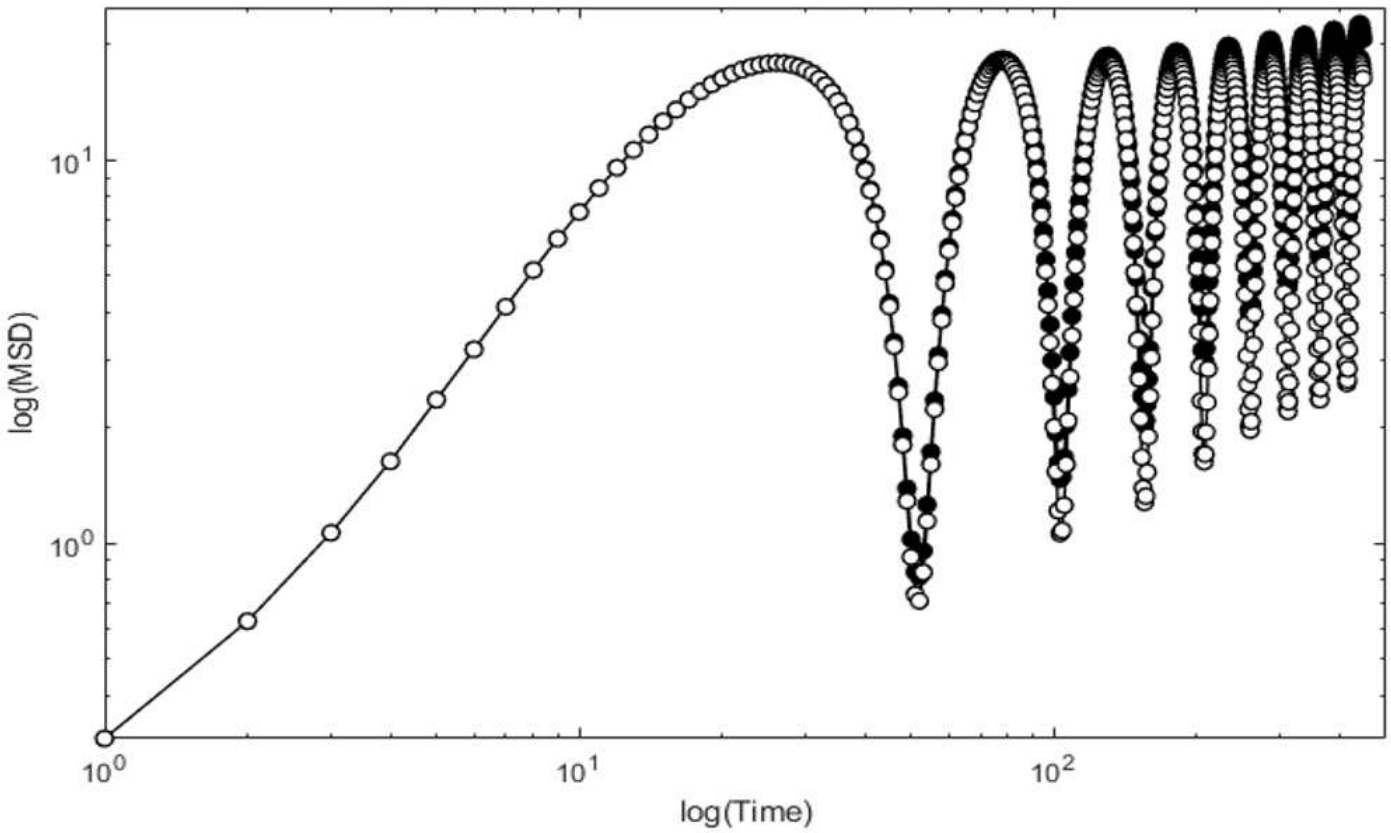

Figure 8

Empirical mean square deviations (MSD) using Eq. (1) for CO2 fluctuations shown in Figure 4 for the quadratic fit (open circles) and linear fit (black circles).

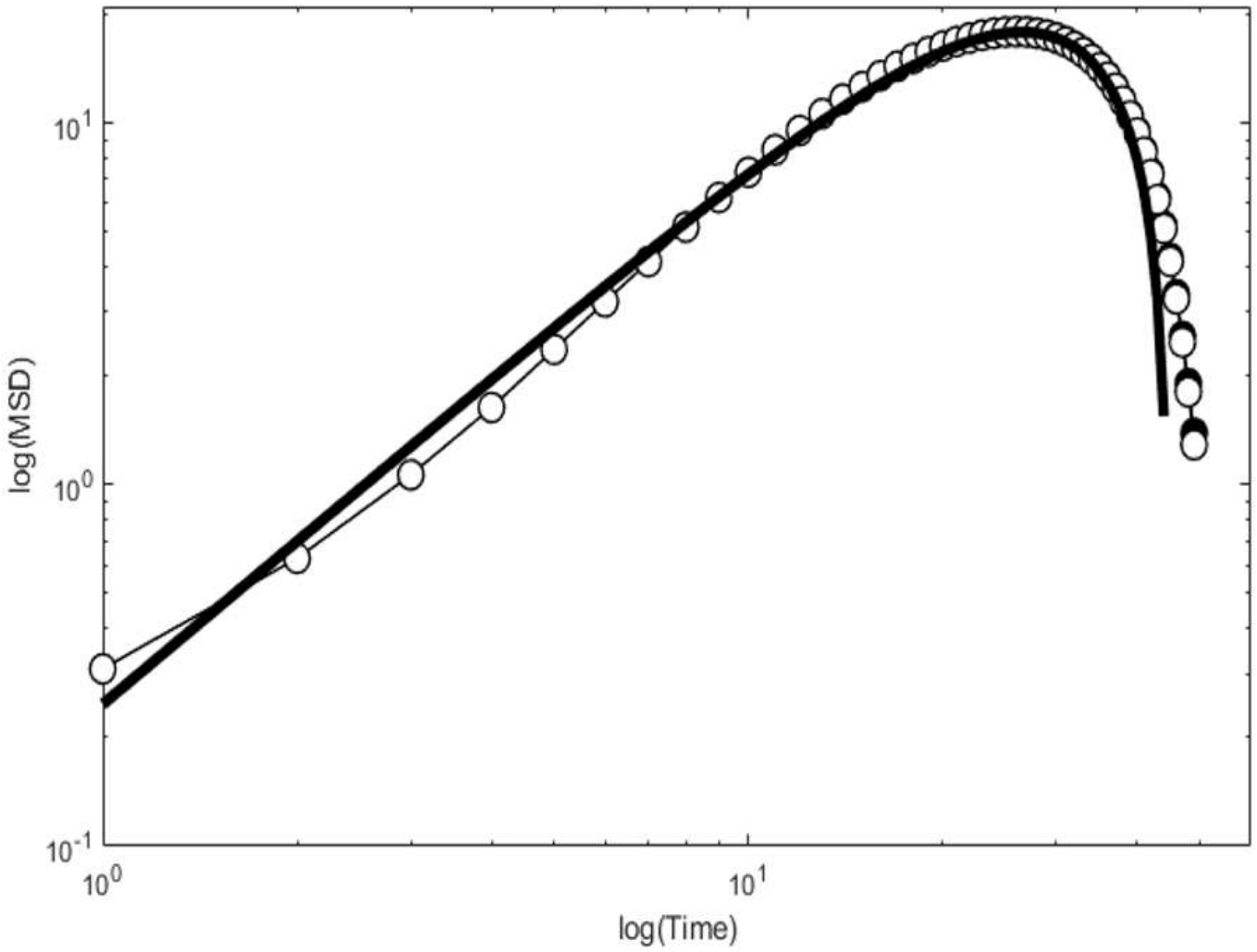

Figure 9

MSD for fluctuations in CO2. Empirical (circles); theoretical (thick solid line) using Eq. (4).

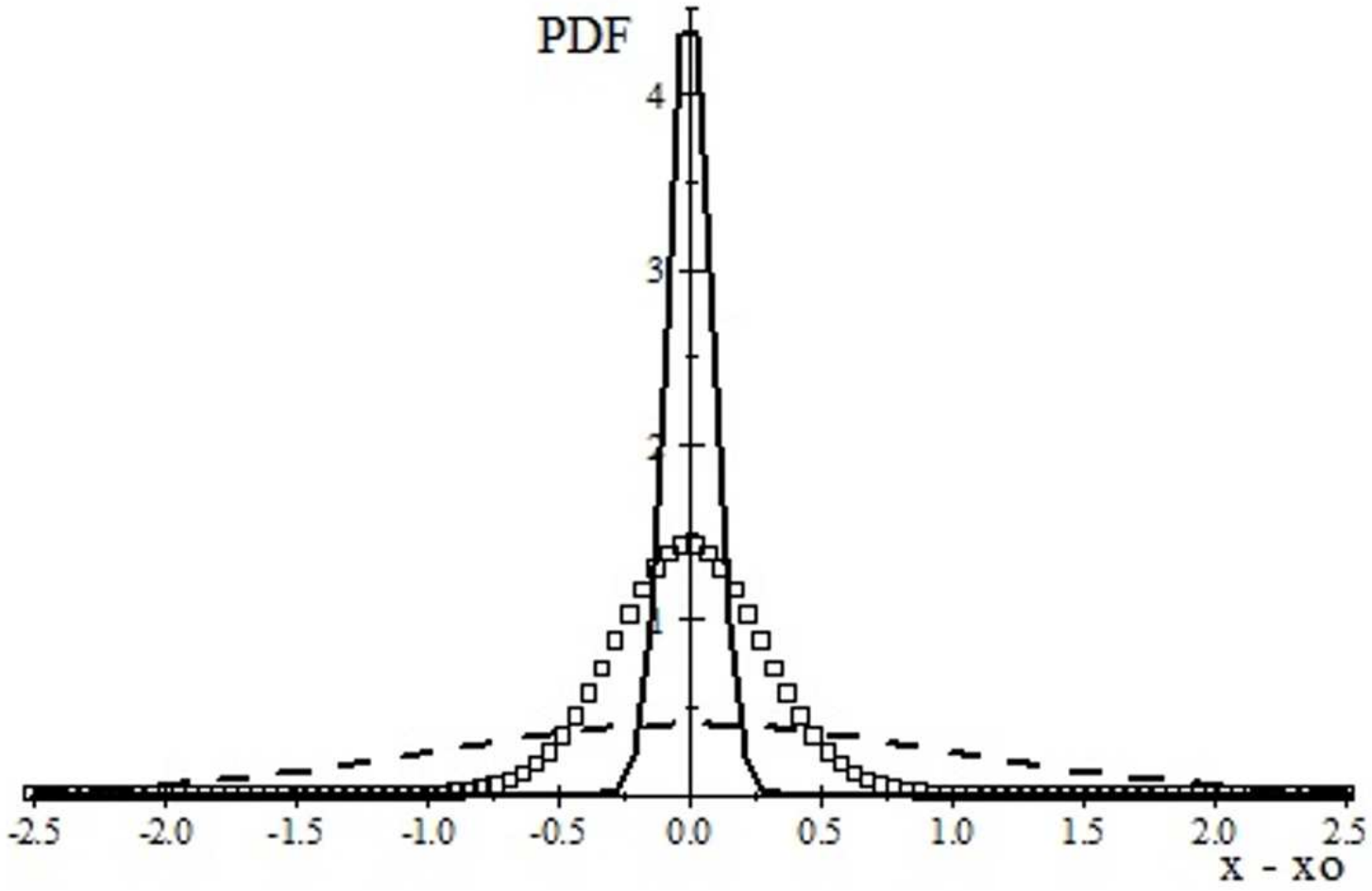

Figure 10

Probability density function for short-time intervals with MSD given by Eq. (7). Subdiffusion (dashed line, α=0.4); superdiffusion (open boxes, α=1.36); hyperballistic diffusion (solid line, α=2.3). All plots are at T=0.2.

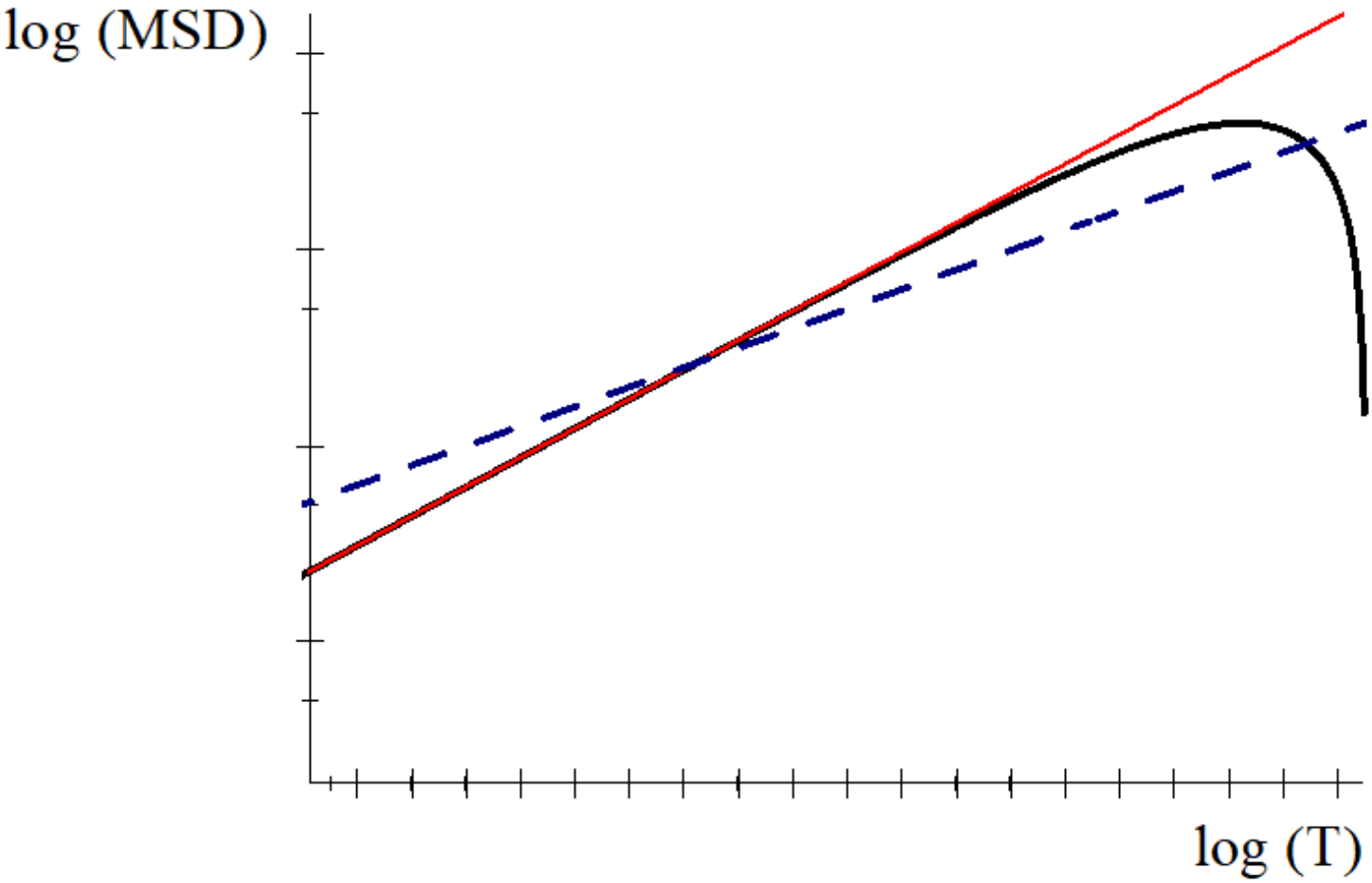

Figure 11

MSD for different memory behavior. Dashed line: Brownian motion (no memory); red straight line: anomalous diffusion; curved black line: stochastic process with memory describing the GBR, CO2 levels, and sea surface temperatures.

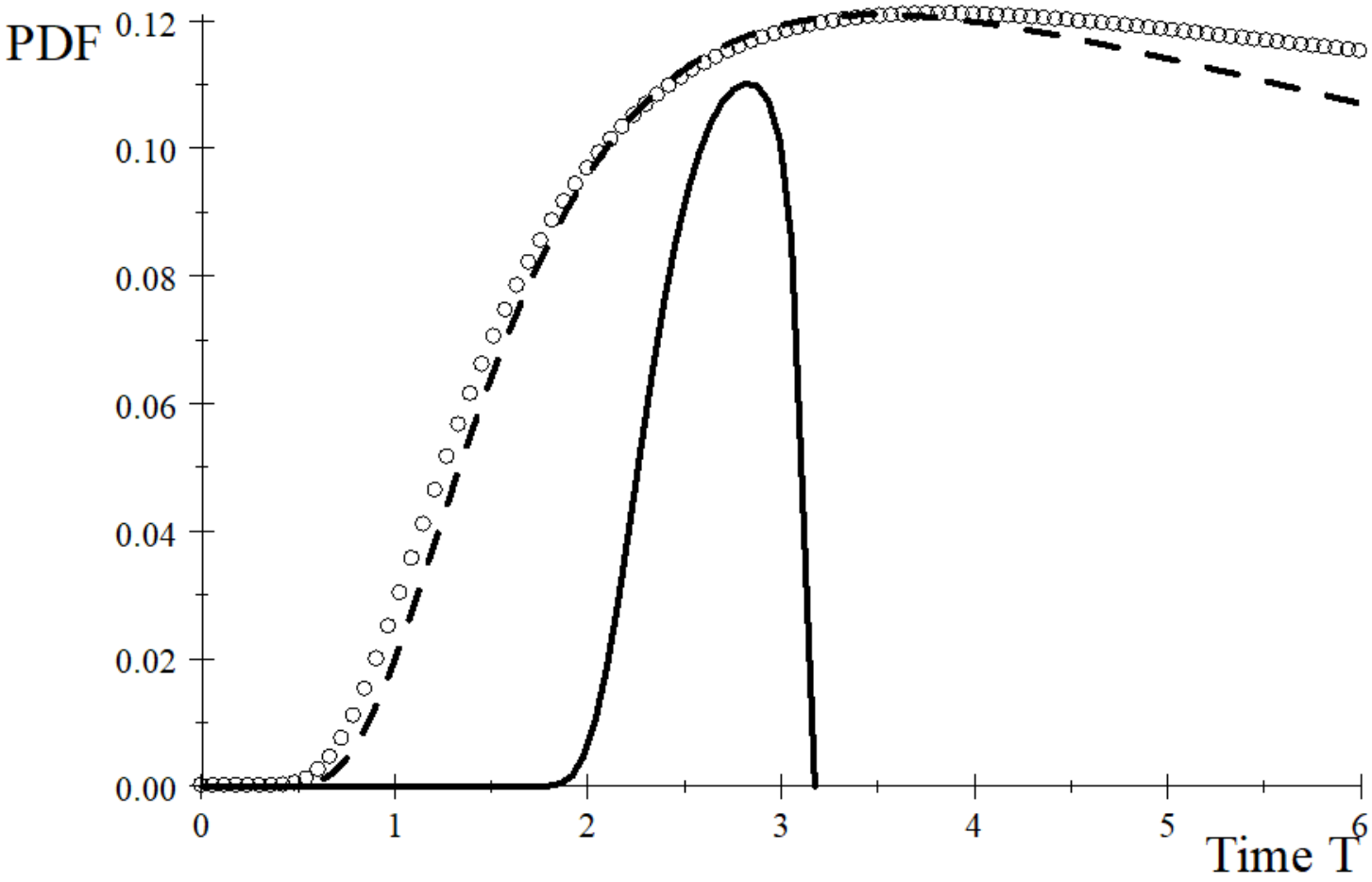

Figure 12

Probability density function (PDF) versus time for the GBR (black solid line, μ=4.64; v=0.99), sea surface temperatures (circles, μ=1.18; v=0.19), and CO2 levels (dashed line, μ=1.25; v=0.07).